Received: 14 March 2022 | Revised: 15 August 2022 | Accepted: 21 September 2022

DOI: 10.1002/stc.3112

RESEARCH ARTICLE

WILEY

Monitoring onsite-temperature prediction error for condition monitoring of civil infrastructures

Mohsen Mousavi[1] | **Amir H. Gandomi**[1] | **Magd Abdel Wahab**[2] | **Branko Glisic**[3]

[1]Faculty of Engineering and IT, University of Technology Sydney, Ultimo, NSW, Australia

[2]Faculty of Engineering and Architecture, Ghent University, Gent, Belgium

[3]Department of Civil and Environmental Engineering, Princeton University, Princeton, New Jersey, USA

Correspondence
Amir H. Gandomi, Faculty of Engineering and IT, University of Technology Sydney, Ultimo, NSW 2007, Australia.
Email: gandomi@uts.edu.au

Abstract

An inverse input–output method is proposed for long-term condition monitoring of civil infrastructures through monitoring the prediction error of air temperature recorded at the site of a structure. It is known that structural natural frequencies are affected by temperature. Hence, the proposed method considers the structural natural frequencies as input and temperature as output to train a machine learning algorithm (MLA). To this end, after signal preprocessing using the variational mode decomposition (VMD), different MLAs are employed, and the error associated with this prediction is regarded as damage–sensitive feature. It is hypothesised and further confirmed through solving numerical and benchmark problems that the prediction error deviates significantly from the upper bond control limit of an R-chart (errors signal) constructed based on the prediction error of temperature as soon as the damage occurs. The frequency–temperature scatter plots indicate a linear dependency between the natural frequencies and temperature. Moreover, the similar slope obtained for the regression line fitted to different frequency–temperature scatter plots indicates high collinearity among pairs of natural frequencies. This observation implies that an interaction term must be considered for such pairs of natural frequencies in the linear regression model. The results of both numerical and experimental studies further confirm that the interaction linear regression model is the most accurate machine learning algorithm for solving the inverse problem of predicting temperature using natural frequencies for condition monitoring of structures. The results of the proposed method are also compared with the direct strategy, whereby its superiority is demonstrated.

KEYWORDS

environmental and operational variations, input–output techniques, machine learning algorithm, regression analysis, structural condition monitoring

1 | INTRODUCTION

Environmental and operational variations (EOV) significantly impact the structural vibration data.[1] It is known that temperature variations can significantly modify structural modal information such as natural frequencies.[2] As a result, a correlation between temperature and the natural frequencies is evident in most of the cases.[3,4] The methods developed for performing long-term condition monitoring of structures under EOV can be divided into (1) output-only methods and (2) input–output methods. The former usually seeks to detect any structural response anomaly without input data caused by damage. At the same time, the latter solves the problem by establishing a map between input and output data and constructing a control chart.[5,6]

It is known that the EOV has nonstationary effects on the structural modal responses, whereas any effect due to damage is stationary. Data normalisation has been widely used to find a stationary representation of the structural modal responses clear from any EOV effects. Since the effect of damage is preserved in the resulting signal,[7–10] condition monitoring of the structure using this signal is made possible without any disturbance caused by the EOV. Cointegration (CI) is a data normalisation technique adapted from econometrics that have been used to perform condition monitoring of various structures.[9–13] However, using CI has sometimes been challenging when a nonlinear dependency between the temperature and structural natural frequencies is evident. Moreover, in some cases, the effect of the EOV on frequencies might be stationary in the long run,[8] which can further challenge the basic unit root assumption of the CI, where it is assumed that the data are nonstationary. Notwithstanding, it was argued that the application of the CI for structural condition monitoring might not be restricted by these shortcomings.[8] Recently, Mousavi and Gandomi[14] proposed a cointegration-based method to resolve the aforementioned challenges. To this end, the variational mode decomposition (VMD) algorithm was first used in a preprocessing stage to denoise and purify natural frequency signals identified through long-term condition monitoring of the structure under study. Next, an LSTM model was trained on the obtained cointegration residuals of the outcome of the VMD to learn underlying principles of the system behaviour under normal (undamaged) conditions. The prediction errors of the cointegration residuals were then taken as damage–sensitive features. There are other output-only methods used to this end, including principal component analysis (PCA),[15,16] time series models,[17,18] and outlier analysis.[19–21] PCA-based algorithms have been widely used for output-only structural condition monitoring. Recently, Mousavi and Gandomi[22] proposed a robust PCA-based algorithm by exploiting the concept of the minimum covarience determinant (MCD)[23] to improve the results of condition monitoring in the Z24 bridge compared to normal PCA. Yan et al[24,25] proposed a PCA-based algorithm applied to structural vibration features identified throughout monitoring the structure under study. The method does not require measured environmental parameters as input as they are taken as embedded variables in the structural characteristics variables. This method's drawback lies in the assumption that the environmental conditions render linear or weakly non-linear effects on the structural vibration characteristics. Sen et al[26] proposed another PCA-based algorithm that takes the magnitude of discontinuity in the principal components of the vibration data as a damage index to be used for quantifying the damage. Hsu and Loh[27] developed a technique based on the nonlinear principal component analysis (NLPCA) and auto-associative neural network. First, some features are extracted that can describe the behaviours of a structure under varying environmental conditions. Then, an auto-associative neural network is constructed to perform prediction on NLPCA of such predictors to be associated with the health condition of the structure. Kalman filter-based algorithms are another class of output-only algorithms that have been used for the condition monitoring of structures. For instance, Erazo et al[28] proposed a technique that is based on this famous property of Kalman filters that the filter is not reflecting optimal conditions when filtering residual cannot be inferred as a realisation of a white stochastic process. As such, any changes in vibration data rendered by environmental variations will not defy the residual from the white process, while this is the other way round when damage occurs.

Several input–output methods have also been developed as a more robust alternative for the long-term monitoring of civil infrastructures. The main reason is the capability of these methods to establish a map between natural frequencies and the EOV effects. Peeters et al. applied ARX models to predict the four lowest natural frequencies of the Z24 bridge using the environmental variables as input.[29] As such, an alarm was proposed to be raised as soon as the predicted natural frequencies are found outside the suggested confidence interval. In another study, Zhou et al.l configured three different back-propagation neural network (BPNN) models that take mean temperatures, effective temperatures, and principal components (PCs) of temperatures as input to individual models to establish the correlation between the modal frequencies and environmental temperatures.[30] The authors used 770h modal frequency and temperature measurement data obtained from the instrumented Ting Kau Bridge to study the effectiveness of the proposed approach. The early stopping technique was employed to avoid over-fitting and enhance the formulated models'

generalisability. The results showed that the BPNN model constructed based on the mean temperatures as input achieves satisfactory performance. Kromanis et al. proposed a methodology based on developing support vector regression (SVR) models to predict the thermal response of a bridge from distributed temperature measurements. Then, they compared the strain predictions obtained from the SVR models with measurements collected from a simulated damaged bridge girder. The errors associated with the predictions are then used for anomaly detection.[31] Reilly et al. monitored the variation of the Coefficient of the Thermal Expansion (CTE) to understand the relationship between the temperature of the structure and the resultant strain and displacement further to monitor structural condition.[32] Ni et al. established mapping between the temperature and modal frequencies using support vector machines (SVMs) to quantify the effect of temperature on modal frequencies.[33] The measurements were separated into the training and validation sets to increase the generalisability of the models. Ceravolo et al. applied time series analysis to find correlations between 10 years of historical environmental data and measurements from static sensors for health monitoring of the Sanctuary of Vicoforte, a monumental Italian church.[34] A review of the methods for condition monitoring of structures under varying temperatures can be found in.[35]

In all the above studies, a direct strategy is followed for anomaly detection based on predicting structural natural frequencies using the EOV effects as input. However, this paper explores the possibility of monitoring temperature prediction error for anomaly detection using structural natural frequencies. Therefore, the proposed method can be considered an inverse approach of its type. To this end, different machine learning algorithms (MLAs) are exploited. The adjusted R-squared metric is employed to assess the performance of the MLAs. The proposed method aims to perform the condition monitoring in a structure (particularly bridges) under the influence of temperature variation through a unique regression model, as opposed to clustering different regression algorithms using the concept of the Schwartz chart. Therefore, it does not require multitype information from EOV effects or additional features from the structure. The only information required is the temperature recorded on the system (bridge deck) and the identified natural frequency signals. We will argue that a linear dependency between the natural frequencies and temperature seems to exist. However, we have also noted the existence of collinearity among the natural frequencies concerning the temperature. All these observations prompt using the interaction linear regression model for solving the indirect regression problem, whose errors are taken as damage–sensitive features. Also, the linear regression's normality assumption for errors justifies using an R-chart for setting a threshold, as this threshold is also obtained based on a similar assumption.

The effect of the EOV on structural vibration data presents some seasonal patterns that do not usually carry any information about the damage. As complex as they are to fit a regression model, it is recommended to exclude them from the vibration data.[36] This is mainly because damage detection algorithms can suffer from the change in the variance of the heteroscedastic data stemming from the effect of the seasonal pattern. Therefore, as a signal preprocessing stage, the complex seasonal patterns were removed from all the signals (i.e., frequency and temperature signals) using the VMD algorithm.[37] VMD was used to denoise and decompose the frequency signals into their constituent components. The mode corresponding to the seasonal pattern was then removed from the signals. The performance of the proposed method is compared against the direct approach to demonstrate its superiority.

2 | THE PROPOSED ANOMALY DETECTION APPROACH

2.1 | Planning the scheme of the method

The flowchart of the proposed method is depicted in Figure 1. In the first step, it is assumed that some information, including a couple of lowest natural frequencies and the air temperature signals, from the healthy state of the structure, are available. Next, following the strategy proposed in Mousavi and Gandomi,[14,23] the VMD algorithm is employed to decompose these signals into the two following intrinsic mode functions (IMFs):

1. IMF_1: A mode that includes information about the long-term dependency between temperature and frequency signals.
2. IMF_2: A mode that represents a short-term dependency between the seasonal temperature fluctuations and the frequency signals.

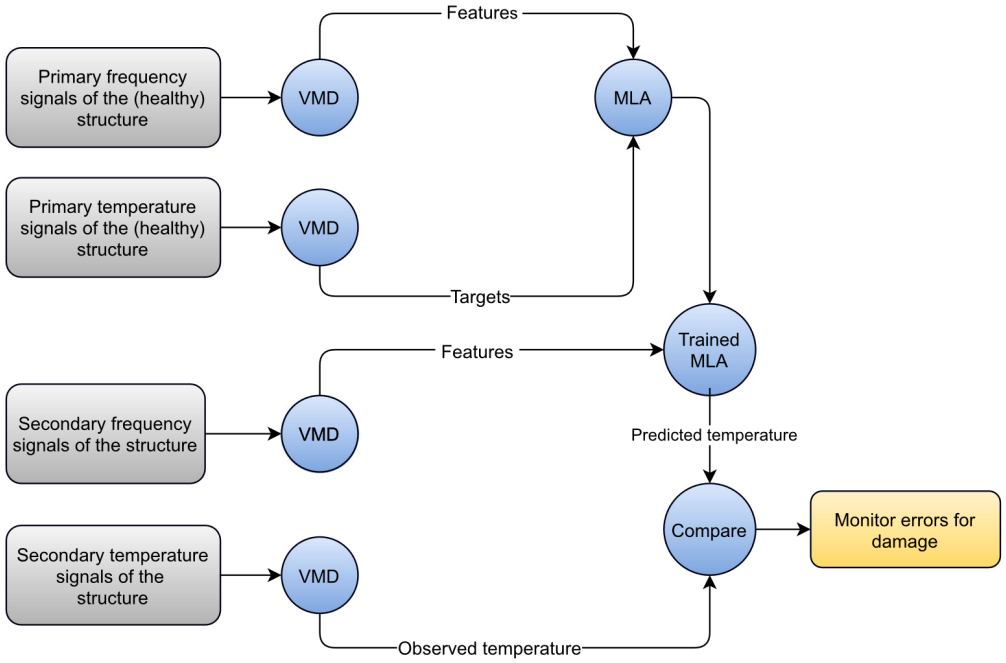

FIGURE 1 Flowchart of the proposed anomaly detection strategy

VMD is used to serve two following reasons: (1) denoising the signals and (2) removing the seasonal patterns (IMF_2) in the signals. Therefore, all IMF_2 signals are excluded from further analysis after decomposing the temperature and frequency signals using VMD.

Next, the obtained IMF_1 signals are used to train a machine learning algorithm (MLA) to learn how to predict the IMF_1 of the temperature signal using those of the frequency signals as input. The trained MLA is then used to predict the future value of the IMF_1 corresponding to the temperature signal using the frequency signals obtained from a posterior state of the structure. Finally, the prediction errors are calculated as the absolute value of the difference between the IMF_1 of the predicted and measured temperature signals.

2.2 | Setting an upper bound threshold

An R-chart is a type of statistical process monitoring scheme used for concurrently monitoring the mean and range of normally distributed variables. Since one of the assumptions of LR models is the normality of error terms (residuals of a regression model), the concept of the R-chart is technically well defined for controlling the range of the prediction errors. We will show that the errors will violate the identified upper control limit (UCL) through the R-chart as the damage occurs in the system.

The errors associated with the temperature prediction can be considered an R-chart, for which one can obtain a UCL based on the historical data. Note that the lower control limit (LCL) is set to zero as the absolute error value is considered a damage–sensitive feature. The UCL is obtained based on the errors obtained from the predictions of the training set as follows:

$$\mathrm{UCL} = D\,\delta\bar{d}_{\mathrm{v}} \tag{1}$$

where $\delta\bar{d}_{\mathrm{v}}$ is the mean value of the obtained R-chart corresponding to the training set. $D = 3.267$ is a constant that depends on the number of variables for which the R-chart is constructed, that is, 2 in here.[38]

2.3 | VMD

VMD is a signal decomposition algorithm typically used for decomposing a nonlinear/nonstationary signal $S(t)$ into its constructive modes. Reiterated, VMD was used in this study for two main reasons: (1) to denoise the signals and (2) to remove the mode corresponding to the seasonal patterns (IMF_2) from the signals. Note that each IMF obtained from VMD decomposition is an amplitude or a frequency modulated signal with the following form[39]:

$$u_k = A(t)\ \cos(\phi(t)) \tag{2}$$

where u_k is the k^{th} mode, $A(t)$ is the instantaneous amplitude, and $\phi(t)$ is the instantaneous phase. VMD solves a variational optimisation problem the procedure of obtaining of which is depicted in Figure 2.

An augmented Lagrangian version of the objective function is constructed to solve the obtained optimisation problem (see Dragomiretskiy and Zosso[39]), which is written as follows:

$$\begin{aligned}\mathcal{L}(\{u_k\},\{X_k\},\lambda) \ &= \alpha \sum_k \left\| \partial_t \left[\left(\delta(t) + \tfrac{j}{\pi t}\right) * u_k(t) \right) \times e^{-ju_k t} \right\|_2^2 \\ &+ \left\| f(t) - \sum_k u_k(t) \right\|_2^2 + \left\langle \lambda(t), f(t) - \sum_k u_k(t) \right\rangle \end{aligned} \tag{3}$$

where λ and α are, respectively, a Lagrangian multiplier and quadratic penalty weight. The alternate direction method of multipliers (ADMM), a sequence of iterative suboptimisation algorithms, is employed to solve the above augmented Lagrangian $\mathcal{L}$ as a saddle point. The readers are referred to the original paper for further details. This makes the VMD a parametric decomposition algorithm, the parameters of which are listed below[40]:

1. k: Sets the number of IMFs into which the signal is to be decomposed.
2. α: Sets the quadratic penalty factor, a denoising term. The immense value of α exerts a more denoising effect on the decomposition process.
3. τ: Determines whether or not the denoising factor α is in effect. A nonzero value of which, for example, 0.1, will secure a more close-to-the-original reconstruction. In this case, denoising is not enforced; thus, the value of α becomes irrelevant.
4. ϵ: Sets the tolerance parameter to control the convergence of the algorithm.

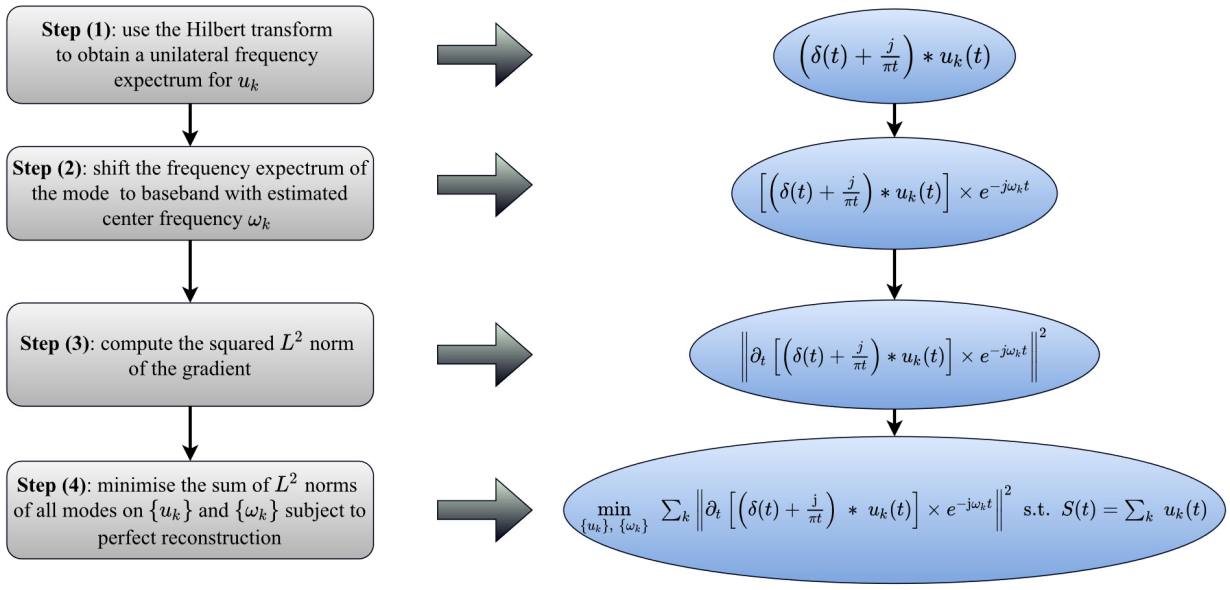

FIGURE 2 The scheme of the VMD. In above diagram, $*$ and j indicate the convolution operator and the imaginary unit, respectively. Also, ω_k is the centre frequency of the k^{th} IMF

5. *init*: Initialises the vector of centre frequencies of IMFs, that is, $\{\Omega\}$. The options are 0, which sets the vector of centre frequencies to the vector of zeros; 1, indicating uniform initialisation where all vector components are the same nonzero value; 2, specifies random values for the vector.
6. *DC*: It is a Boolean parameter and determines whether or not the first IMF is kept at zero centre frequency. The options are 1 for true and 0 for false.

For further information about the VMD algorithm, the readers are referred to the original paper.[39] The readers are also referred to the computer program of the VMD developed by its proposers as in reference.[40] Further information about how to specify the VMD parameters can be found in Mousavi and Gandomi.[14,23]

2.4 | Machine learning algorithms

The regression learner toolbox in MATLAB was used to solve the problem. There are five groups of MLAs, which are as follows: (1) Linear regression (LR), (2) Trees, (3) Support Vector Machine (SVM), (4) Gaussian Process Regression (GPR), and (5) Ensemble of trees. Table 1 lists all the MLAs employed in this paper.

Next, a metric is presented to evaluate the effectiveness of each ML model for predicting temperature using structural natural frequencies.

2.5 | Effectiveness of a model

It is essential to know how much of the total variance of the target outcome is explained by the developed ML model. To this end, a metric termed R-squared can be used, which is defined as follows:

$$R^2 = 1 - \frac{\mathrm{SSE}}{\mathrm{SST}} \tag{4}$$

where the terms SSE and SST are, respectively, the squared sum of the errors and the squared sum of the data variance calculated as follows:

$$\mathrm{SSE} = \sum_{i=1}^{n} \left(y^{(i)} - \hat{y}^{(i)}\right)^2 \tag{5}$$

$$\mathrm{SST} = \sum_{i=1}^{n} \left(y^{(i)} - \bar{y}\right)^2 \tag{6}$$

in which $y^{(i)}$, $\hat{y}^{(i)}$, and $\bar{y}$ denote the vectors of observed target values, predicted target values, and the average of the observed target values, that is, temperature in this paper, respectively. Also, n denotes the number of observations. SSE explains how much variance remains after fitting the model, whereas SST is the total variance of the target outcome.

TABLE 1 MLAs employed to create the anomaly detection method in this paper

Linear regression	Trees	Support vector machine	Gaussian process	Ensembles of trees
Normal linear	Fine tress	Linear SVM	Rational quadratic	Boosted trees
Interaction linear	Medium trees	Quadratic SVM	Squared exponential	Bagged trees
Robust linear	Coarse trees	Cubic SVM	Matern 5/2	
Stepwise linear		Fine Gaussian	Exponential	
		Medium Gaussian		
		Coarse Gaussian		

Typically, the value of R^2 ranges between 0 and 1, representing the case when the model does not explain the data and for the model that explains all of the variances in the data, respectively. The higher value of R^2 thus indicates that the model describes the data better. As such, the R^2 value is a metric to compare the fitness of the chosen model with that of a horizontal straight line. Note that the horizontal straight line is considered the null hypothesis. A negative value for $\overline{R}^2$ may be obtained when the model performs worse than the horizontal straight line.

It is argued that the value of R^2 increases with the number of features in the model.[41] This is not, however, always meaningful as some features might not contain any information about the target value. As such, another metric termed adjusted R-squared is usually used instead, which is defined as follows:

$$\overline{R}^2 = 1 - (1 - R^2)\,\frac{n-1}{n-p-1} \tag{7}$$

where p and n indicate respectively the number of predictors (features) and the number of observations.

Likewise, to R^2, a model with a shallow $\overline{R}^2$ does not explain much of the variance and, therefore, is not interpretable. As such, any interpretation of the weights (the regression model coefficients) would not be meaningful. Moreover, the R^2 value increases as more variables (features) are used in the model. This may well convince the user that increasing the number of variables will favour the fitness of a model. However, some variables might not be helpful in capturing the variance in the model. As such, $\overline{R}^2$ can be used to interpret the reliability of a model regardless of the number of variables used in the training stage. It can also be used to decide whether adding a variable can improve the fitness of a model.

Next section solves a numerical example of a spring-mass system using the proposed condition monitoring approach.

3 | SELECTION OF AN APPROPRIATE MODEL

3.1 | A numerical example of spring-mass system

A four degrees of freedom (4-dof) spring-mass system is studied in this section as an illustrative example. The motivation behind selecting such a model comes from a similar example studied in Shi et al.[42] This model selection also makes it compatible with the benchmark problem of the Z24 bridge, where only the first four natural frequencies are available. Moreover, the stochastic subspace identification method is usually used to identify the natural frequencies from historical vibration data. However, according to Moaveni and Asgarieh,[43] the identification errors for the higher order natural frequencies increases. Therefore, they are preferred not to be used for condition monitoring in this study. Figure 3 depicts the picture of the spring-mass system. The masses weigh 2 kg each. The stiffness of each spring, in kN/m, is assumed to vary with temperature according to the following equations:

$$k = \begin{cases} -0.11 \times (T-15) + 4, & \text{if } T < 15 \\ -0.03 \times (T-15) + 4, & \text{if } T \geq 15 \end{cases} \tag{8}$$

and

$$k^* = \begin{cases} -0.11 \times (T-15) + 5, & \text{if } T < 15 \\ -0.2 \times (T-15) + 5, & \text{if } T \geq 15 \end{cases} \tag{9}$$

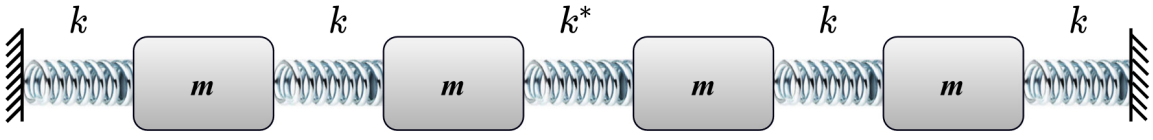

FIGURE 3 A 4-degree-of-freedom spring-mass system

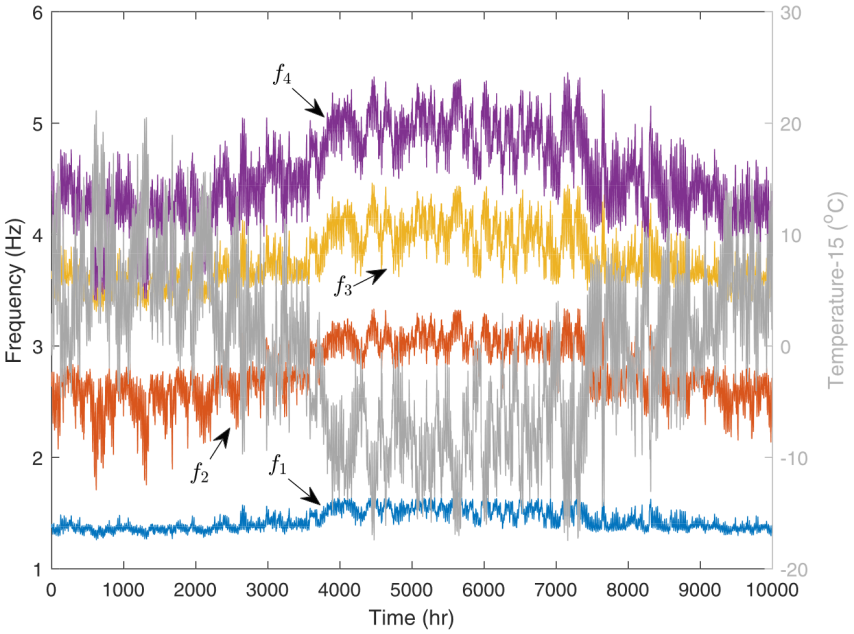

FIGURE 4 Right-to-left: Hourly recorded temperature of Basel-Switzerland shifted −15°C, and left-to-right: calculated natural frequencies of the damaged spring-mass system for the time period from June 2019 to July 2020

The different behaviour of k^* exerts nonlinear effects on the vibration modes. The right-to-left plot of Figure 4 shows an hourly recorded temperature profile in Basel-Switzerland from June 2019 to July 2020, which was used to obtain the stiffness of the springs at each time instant, using (8) and (9). The data for the temperature profile can be found in a previous work.[44]

It is assumed that the stiffness of k^* reduces by 5% at 8000^{th} record. Also, this stiffness reduction lasts until the recording time's end. This reduction is considered an anomaly to be detected by the MLAs. The four natural frequencies of the system were calculated by solving the generalised eigenvalue problem of

$$\left|M-\omega^2 K\right|=0 \tag{10}$$

where M and K are, respectively, the mass and stiffness matrices of the spring-mass system.

The obtained frequency signals are contaminated by 10% noise to simulate the scenario of noisy frequency signals. The following equation is used to this end[45]:

$$\hat{\delta}=\delta+\frac{\kappa}{100}n_{\text{noise}}\sigma(\delta) \tag{11}$$

where δ and $\hat{\delta}$ represent respectively the vector of clean and noisy frequencies, $\sigma(\delta)$ indicates the standard deviation of δ, κ is the noise level $(=10)$, and n_{noise} is a random independent variables vector of the same size, and δ is simulated to follow a standard normal distribution.

Note that the parameters of the spring-mass model of this paper are comparable to a similar example studied in Shi et al,[42] where a 2% noise and 20% damage were considered in simulations.

The Left-to-Right plot of Figure 4 shows the spring-mass system's four noisy natural frequency signals. Figure 5 shows the scatter plot of the natural frequencies versus temperature. The figure indicates the linear dependency between the temperature and natural frequencies. These linear dependencies, however, change pattern when the temperature is shifted by −15°C. A linear regression model thus can best characterise the dependence between the natural frequencies and temperature.

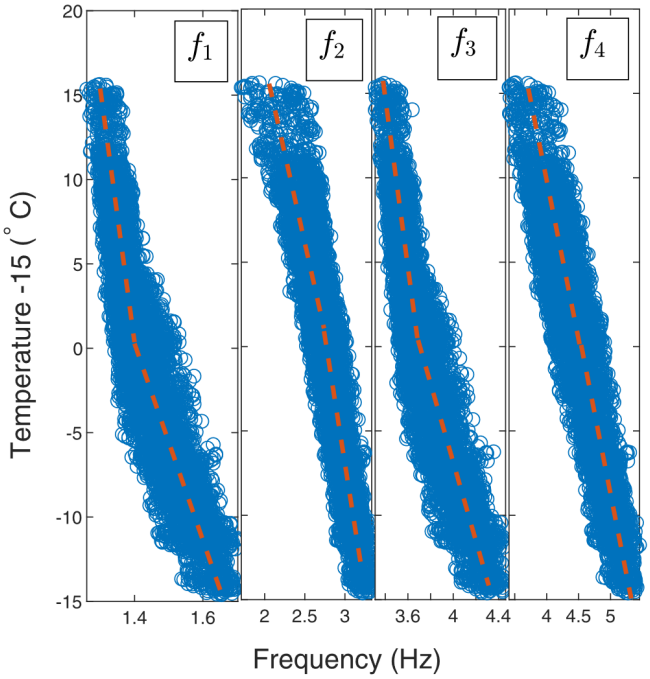

FIGURE 5 The scatter plot of the temperature versus natural frequencies of the spring-mass system

Moreover, the similar slopes of the line fitted to each scatter plot indicate the existence of collinearity among variables. Therefore, a to-be-developed regression model must consider interactions among the natural frequencies. Consequently, we hypothesise that a linear regression model with interaction terms best characterises mapping between the natural frequencies and temperature. This hypothesis will be further tested by employing different MLAs to solve the regression problem of this section.

The four natural frequencies and the temperature signals are decomposed into IMF_1 and IMF_2, that is, a DC mode and the mode corresponding to the seasonal patterns in the signals, respectively. τ was set to zero, and the quadratic penalty term was set at 100, that is, $\alpha = 100$ to have denoising effects in the decomposition process. Below, it is explained how the value of α was selected:

The decomposition results of the temperature signal and the natural frequencies along with the IMFs' centre frequencies are shown respectively in Figures 6 and 7. As can be seen from the figures, a zero centre frequency was obtained for all the first IMFs. Regarding the natural frequencies signals, the average centre frequency of the second IMFs is about 0.0439 cycles per hour,* almost a full cycle per 24 h. This follows that the temperature variations between day and night show a cyclic pattern throughout the year. Note that any values larger or smaller than $\alpha = 100$ will not bear such results regarding the centre frequencies of the second IMFs. All IMF_1 signals were then used for training the MLAs.

Next, the outcomes of the VMD were divided into three parts: 40% of the data was used for training, 30% for validations, and the remaining 30% for testing. The first 4000 records of all IMF_1 signals were thus used for training the MLAs of Table 1.

Figure 8 shows the calculated $\overline{R}^2$ of the predictions using the MLAs made on the validation set. It can be generally seen that, among all the MLAs, the linear regression (LR) models best confirm the hypothesis made earlier. This observation is also compatible with the plots in Figure 5, which indicate a linear relationship between the natural frequencies and temperature. Next, the best model within each category was selected based on its performance, and the prediction results are presented in Figure 9. Note that the dashed red line indicates the time of damage initiation. The selected models are as follows: (1) interaction LR, (2) fine trees, (3) linear SVM, (4) squared exponential GPR, and (5) bagged trees. Although the interaction LR and stepwise LR equally perform well, the stepwise linear is not recommended due to several reasons that are reported in Flom and Cassell.[46] Therefore, the results of the interaction LR are only presented here. The relatively better performance of the interaction LR for damage detection is due to the interaction among natural frequencies, as identified in the plots of Figure 5. The number of data points in the training set is also enough for fitting a perfect model on the data. It is worth noting that poor fitness might be achieved if the

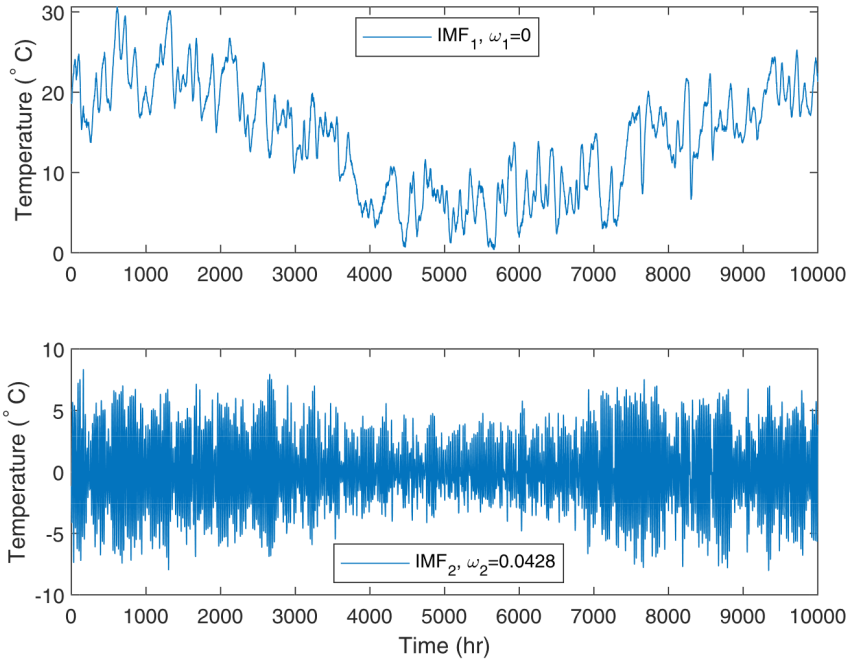

FIGURE 6 IMFs of the decomposed temperature signal of the spring-mass system along with their centre frequencies. The first IMF is kept at DC (zero centre frequency)

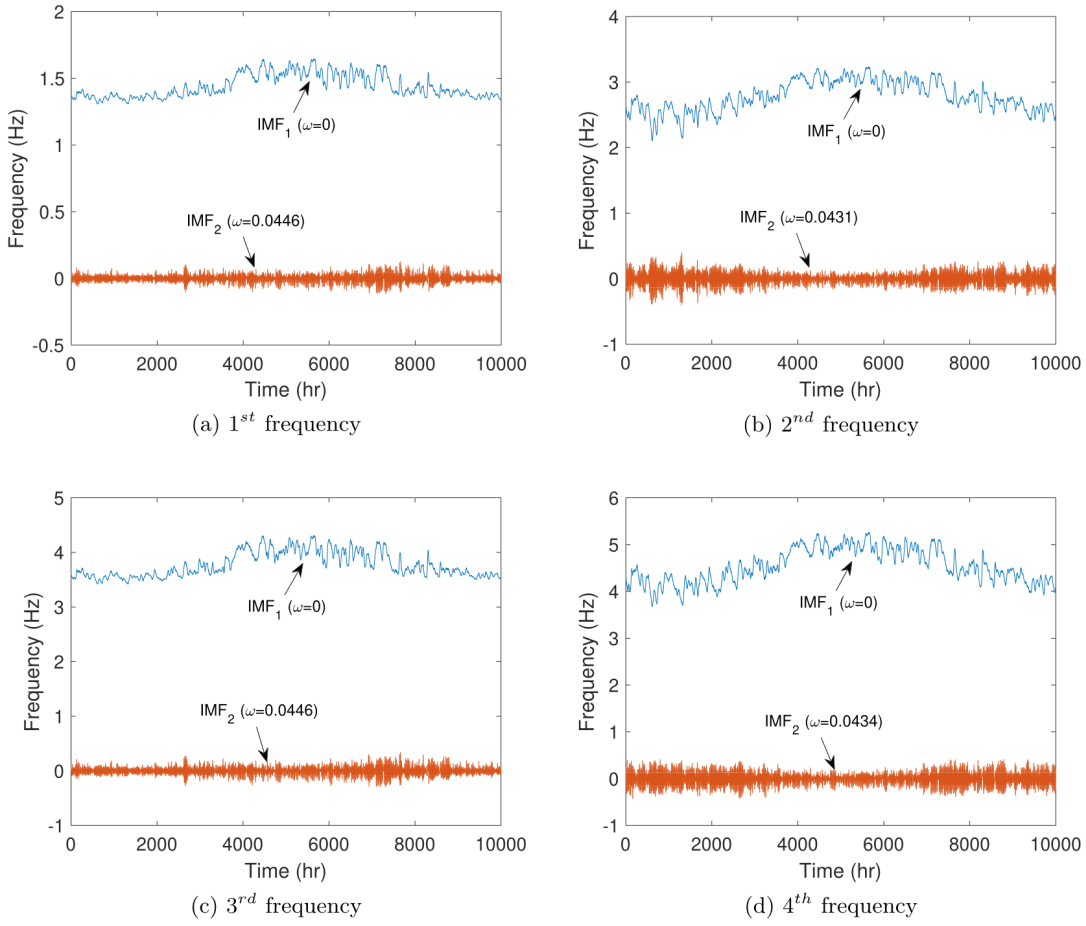

FIGURE 7 Decomposed natural frequencies of the damaged spring-mass system along with their centre frequencies. The first IMF in all cases is kept at DC (zero centre frequency)

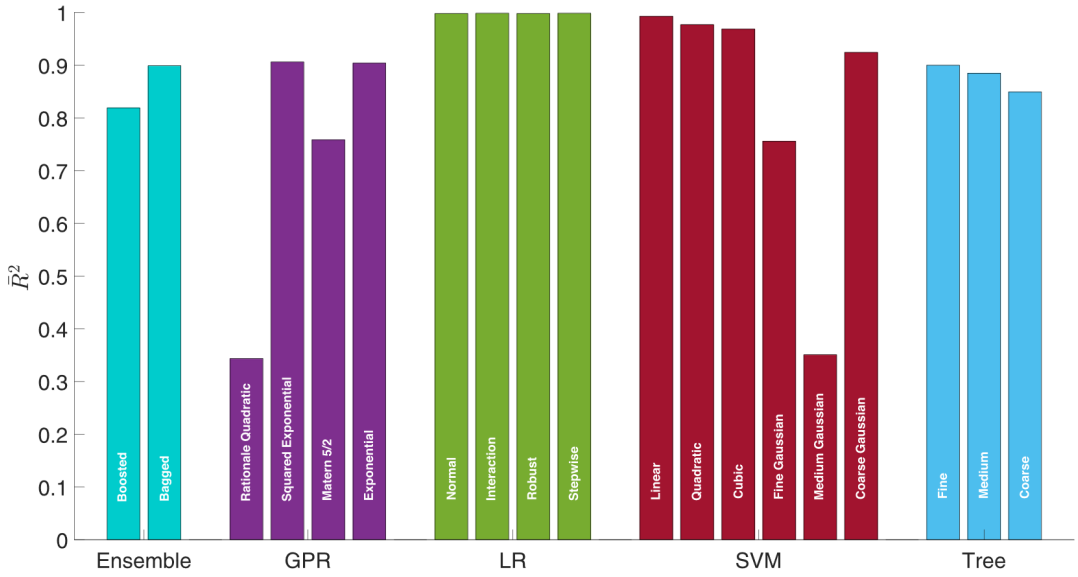

FIGURE 8 Calculated $\bar{R}^2$ on the validation set using different MLAs regarding the spring-mass system

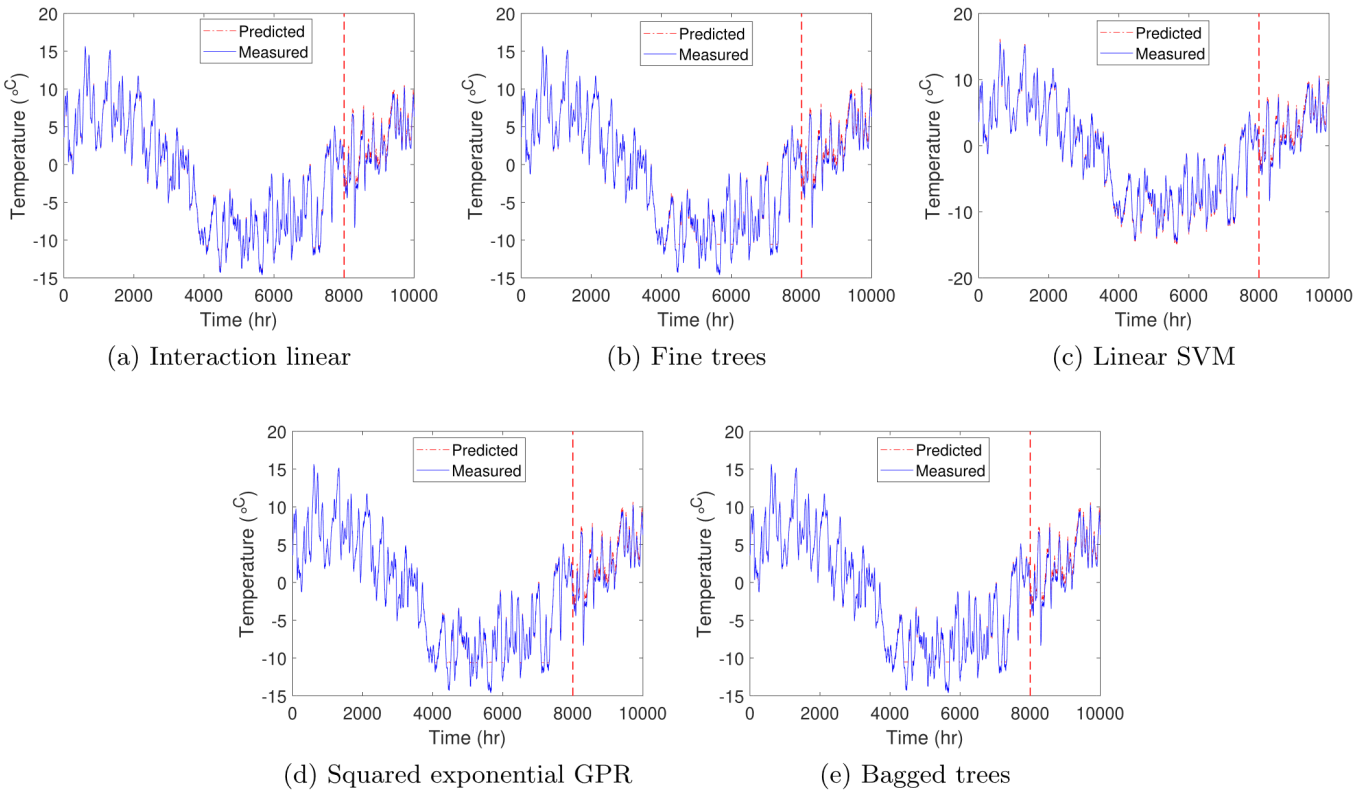

(a) Interaction linear (b) Fine trees (c) Linear SVM

(d) Squared exponential GPR (e) Bagged trees

FIGURE 9 The predicted and measured temperatures regarding the spring-mass system using different trained MLAs

training set is not large enough. We will show later in the experimental study section this is the case. In summary, the better performance of the LR model in the example of the spring-mass system is for the two following reasons:

1. First and foremost, the linear dependency between the natural frequencies and temperature, evident from Figure 5, justifies the LR models' better performance compared to the other MLAs.
2. The existence of collinearity among the natural frequency signals prompts using the interaction terms in the LR model.

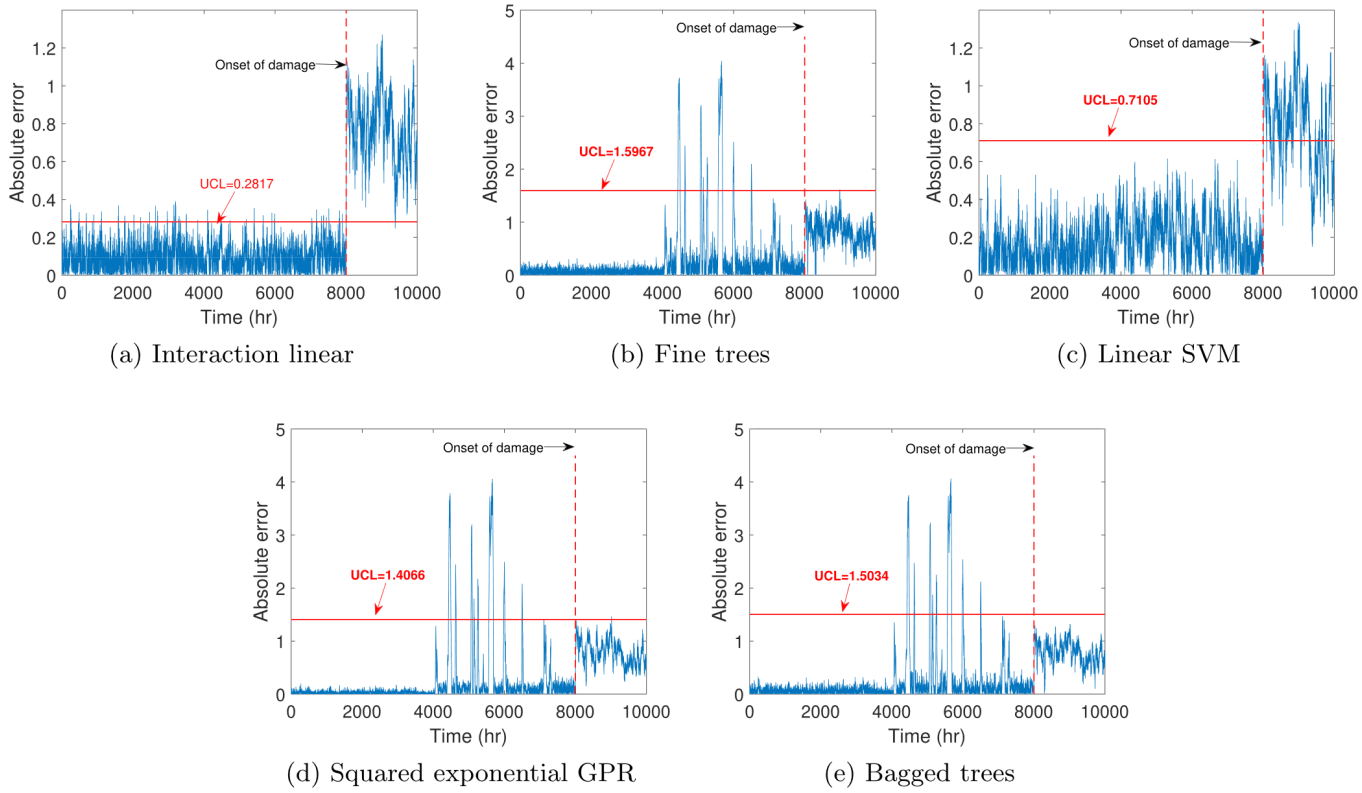

FIGURE 10 Condition monitoring results of the spring-mass system using different trained MLAs (note differences in scale of y-axis in graphs)

3. The number of data points in the training set is enough for a model to be perfectly fitted to the data.

Figure 10 shows the errors in prediction associated with each selected MLA. The UCL for each case was obtained based on Section 2.2. As can be seen from the figures, the interaction LR and linear SVM models perform best among all the other models, as expected. However, considering the UCL as a threshold, the interaction LR is way more accurate than the linear SVM. Therefore, the results of the numerical example of this section suggests the selection of the interaction linear model due to the following reasons:

1. The interaction LR model performs best in anomaly detection and model fitness compared with all the other MLAs.
2. Compared with other MLAs, the interaction LR model is more straightforward and does not require any hyperparameters tuning, making it easy to interpret.

Next, a brief explanation of the LR models is presented to understand better why interaction LR performs better than other linear models such as ordinary LR.

3.2 | Linear regression models

3.2.1 | Normal linear regression

The formula of the ordinary LR model, regarding the problem of the previous section (with four variables), can be described as follows:

$$T = \beta_0 + \beta_1 f_1 + \beta_2 f_2 + \beta_3 f_3 + \beta_4 f_4 + \epsilon \tag{12}$$

where β_0 is the weight associated with the intercept and $\beta_i, i = 1, ..., 4$ are the weights corresponding to the i^{th} feature (natural frequency). Note that ϵ is the error term.

Various methods can be used to estimate the values of the weights, the most common type of which is the ordinary least squares method (LSM). As such, the LSM seeks to find the weights that minimise the squared differences between the actual observations and the estimated outcomes as follows:

$$\hat{\beta} = arg\min_{\beta_0,\ldots,\beta_p} \sum_{i=1}^{n} \left(y^{(i)} - \left(\beta_0 + \sum_{j=1}^{p} \beta_j x_j^{(i)} \right) \right)^2 \tag{13}$$

where in this study, $p = 4$ and n denotes the number of observations (the frequencies and temperature records). The readers are referred to Friedman et al[47] for further information about how the weights of (12) can be obtained.

3.2.2 | Robust linear regression

The least squares estimates of (12) are susceptible to outliers—the observations that do not follow the pattern of the other observations. Reiterated, one of the main assumptions behind normal LR is "Homoscedasticity" of the datasets. Homoscedastic model implies that the variance of the error term is constant in all instants. However, in some cases that there is a strong suspicion of "Heteroscedasticity" (the opposite of Homoscedasticity), the robust regression may be used. Heteroscedasticity implies that the variance is dependent on variables.

3.2.3 | Interaction linear regression

In some cases, adding an interaction term (cross-product term) regarding two independent variables improves prediction results, enabling the explanation of nonlinearity in the established map. In such a case, the modified version of (12) is obtained as follows:

$$\begin{aligned} T \; &= \beta_0 + \beta_1 f_1 + \beta_2 f_2 + \beta_3 f_3 + \beta_4 f_4 + \beta_5 f_1 f_2 + \beta_6 f_1 f_3 \\ &+ \beta_7 f_1 f_4 + \beta_8 f_2 f_3 + \beta_9 f_2 f_4 + \beta_{10} f_3 f_4 + \epsilon \end{aligned} \tag{14}$$

where the term $f_i f_j$ characterises the nonlinear effect on T caused by the interaction between f_i and f_j.

3.2.4 | Step-wise linear regression

Consider the interaction linear regression model of (14). Step-wise LR is a method that performs a statistical model test for each predictor step-wise to insert the predictor into the model and keep it if it "improves" the model. Sometimes, an opposite procedure can also be applied. As such, all the candidate variables are first included in the model. Then, the elimination of each variable is tested using a chosen model fit criterion. As such, variables whose elimination results in the most statistically insignificant deterioration of the model fit are removed from the model. Also, a mixture of the above approaches can be followed where the variables are either included or excluded in each step. Reiterated, while step-wise LR might perform well in some cases, its usage is not preferable due to several reasons reported in Flom and Cassell.[46]

Regarding the above short descriptions of the LR models, one can conclude that both interaction and step-wise LR models can capture nonlinear dependency between the attributes and target. Since different behaviour of spring k^* introduces nonlinearity to the vibration of the spring-mass system, the better performance of the interaction and step-wise LR models is somewhat justified.

Next, the importance of each independent feature and the interaction terms of the interaction LR model obtained for the spring-mass system is investigated.

3.3 | Feature importance

The importance of each term in a linear model can be represented by the value of the *t*-statistic, which, in its general form, is the difference between the estimated weight and its actual value scaled with its standard error shown as follows:

$$t_{\hat{\beta}_j} = \frac{\hat{\beta}_j - \beta_{0j}}{SE\left(\hat{\beta}_j\right)} \tag{15}$$

where $\widehat{\beta}_j$ and β_{0j} are respectively the estimated weight and its hypothesised value and $SE\left(\hat{\beta}_j\right)$ denotes the standard deviation errors of the estimator $\widehat{\beta}_j$.

Knowing how much each term in the interaction LR model of (14) contributes to estimating the temperature in the obtained LR models of the spring-mass system helps assess model validity. This can be achieved by setting $\beta_{0j} = 0$ in (15) and obtaining the absolute value of the t-statistic corresponding to the linear regression model[41] as follows:

$$\bar{t}_{\hat{\beta}_j} = \left| \frac{\hat{\beta}_j}{SE\left(\hat{\beta}_j\right)} \right| \tag{16}$$

By closely investigating (16), one can conclude that the importance of a feature increases with increasing the estimated weight $\widehat{\beta}_j$. Furthermore, the more significant variance of the estimated weight implies less certainty about the predicted value or, equivalently, less importance of the feature.

Table 2 shows the parameters of the trained interaction LR model for the spring-mass system. The "Feature" column indicates the intercept as well as all the four features and the mutual interaction terms between each pair of features. The column "Weight" shows the estimated weights β_0 to β_{10} as in (14). The following is the short description of each term in the table:

- SE represents the standard error of the estimated weights $\widehat{\beta}_j$.
- $\bar{t}_{\hat{\beta}_j}$ represents the *t*-statistics as presented in (16).
- *p* value tests the null hypothesis of each coefficient being equal to zero (no effect). A low *p* value (<0.05) indicates that one can reject the null hypothesis. The coefficient *p* values can determine which terms should be kept in the regression model. Therefore, one may expect a correlation between the *t*-statistic and *p* value regarding each term in the LR model.

TABLE 2 Parameters of the interaction LR model regarding the spring-mass system

Feature	β	Weight	SE	$\bar{t}_{\hat{\beta}_j}$	*p* value
Intercept	β_0	90.16192	2.3259	38.7643	0
f_1	β_1	74.6096	13.1763	5.6624	0
f_2	β_2	−8.1528	6.2382	1.3069	0.1913
f_3	β_3	27.4213	4.9675	5.5201	0
f_4	β_4	−61.6271	3.0225	20.3892	0
$f_1\&f_2$	β_5	−55.1649	31.3247	1.7611	0.0783
$f_1\&f_3$	β_6	−74.2382	3.9931	18.5917	0
$f_1\&f_4$	β_7	77.4536	20.9266	3.7012	0.0002
$f_2\&f_3$	β_8	36.7464	12.0881	3.03989	0.0024
$f_2\&f_4$	β_9	−13.6135	0.6231	21.8493	0
$f_3\&f_4$	β_{10}	−5.5577	7.9309	0.7008	0.4835

The results of the Table 2 indicate that f_4 is the most important independent feature with $\bar{t}_{\hat{\beta}_j} = 20.3892$. Accordingly, f_1 is the second most important independent feature with $\bar{t}_{\hat{\beta}_j} = 5.6624$. It can be seen that f_2 is of the least importance among all the four independent features. Note that the obtained large p value $= 0.1913$ for f_2 also confirms its minor contribution to the temperature prediction in the regression model. Regarding the interaction terms, interestingly, the interaction between f_2 and f_4 is of the greatest importance ($\bar{t}_{\hat{\beta}_j} = 21.8493$), although the importance of f_2 alone is of the least. The second most important interaction effect goes to the pair $f_1\&f_3$ with $\bar{t}_{\hat{\beta}_j} = 18.5917$. One reason could be the similar slope of these natural frequencies' dependency on the temperature. As evident from Figure 5, the slopes of the pairs $f_1\&f_3$ and $f_2\&f_4$ are pretty similar, reflecting the collinearity of these pairs. The existence of the collinearity between two variables indicates that they cannot independently predict the target values, further confirming the importance of the interaction terms in the model.[48] Note that the least important interaction term $f_3\&f_4$ has also a large p value of 0.4835. Therefore, statistical analysis has shown that in the spring-mass system's specific case, the following features have the most significance: Interaction between f_2 and f_4, f_4, and interaction between f_1 and f_3.

3.4 | Significance of using VMD

We have seen so far that the nonlinear dependency between temperature and frequencies can be well captured by the interaction terms added to the LR model. In this section, we continue to use the interaction LR model and compare its results with and without the application of the VMD. Next, larger values of α are used to impose more severe denoising effects on the features and targets obtained to investigate possible effects on condition monitoring results.

Figure 11 shows the results of the condition monitoring with (Figure 11a) and without (Figure 11b) employing the VMD for denoising and removing the seasonal patterns. It is evident from the results that the application of the VMD is crucial in this case. We show later that this is also the case for the benchmark problem of the Z24 bridge.

Next, larger values of α were used to investigate its effect on the condition monitoring results. Figure 12a,b shows the prediction results of the interaction LR model when α was set at 1000 and 10,000, respectively. The difference between the two obtained "Measured" signals in the graphs is due to the various denoising effects imposed by different values of α in the VMD settings. Note that the IMF_2 signals corresponding to the seasonal patterns have been excluded before conducting the regression analysis.

Figure 13a,b shows respectively the obtained prediction errors along with the calculated UCL for the interaction LR models. Reiterated, the performance of the models can be evaluated using $\bar{t}_{\hat{\beta}_j}$. As such, a slightly smaller values of $\overline{R}^2$ were obtained for the cases of $\alpha = 1000$ and $\alpha =$ 10,000. However, the model's performance in anomaly detection is not much affected by the value of α.

To summarise the above observations, the trained MLA model must fulfil the two following conditions:

1. Since the model is trained on data from the healthy structure, it must be generalisable to the case when the system remains intact.
2. The developed model must not be generalisable to the case when damage occurs in the system.

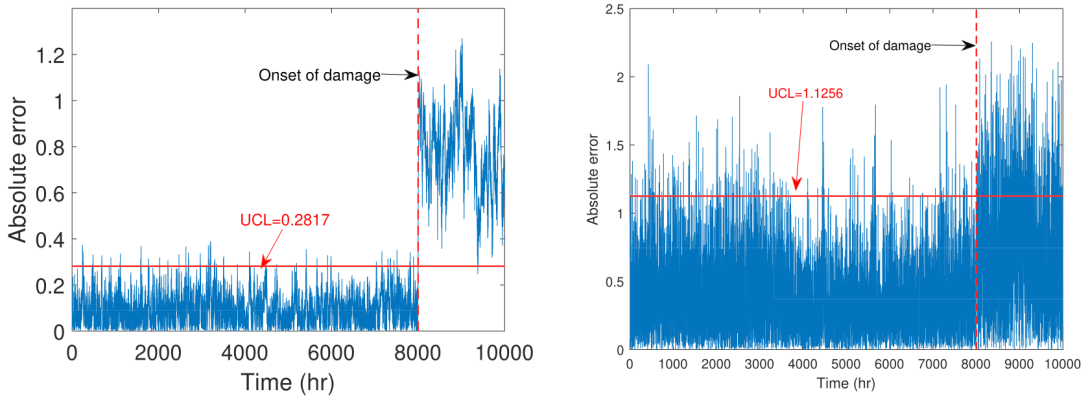

(a) With VMD (b) Without VMD

FIGURE 11 Condition monitoring results of the spring-mass system with and without application of the VMD

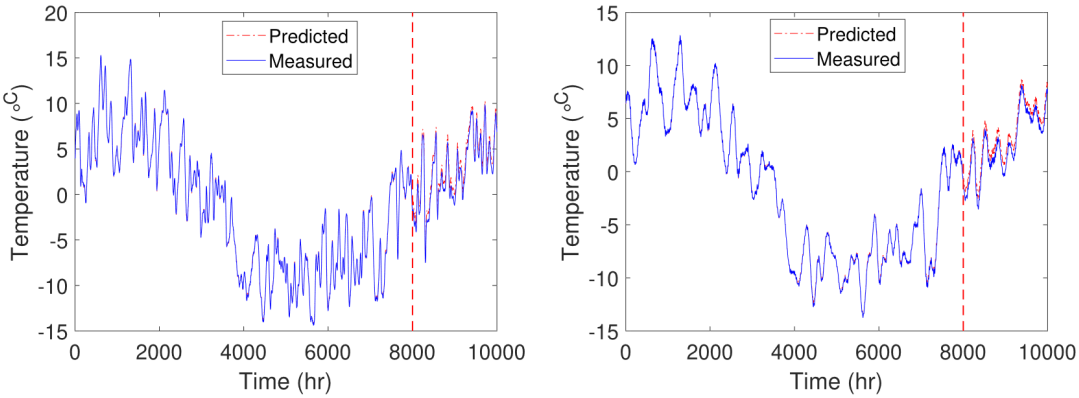

FIGURE 12 Prediction results of interaction LR model using different α in the VMD settings

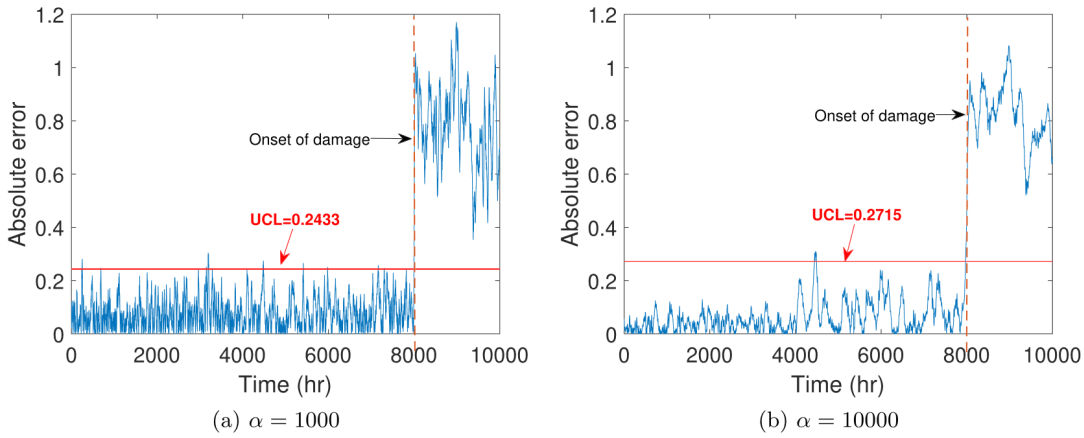

FIGURE 13 Obtained errors from application of the interaction LR model using different α in the VMD settings

As such, the interaction LR model is found to be the best model that fulfils the two conditions mentioned above. Although some false-negative/positive observations are evident in the interaction LR results (Figure 10a), these observations are primarily due to the introduced excessive noise to the data. To clarify this, we would like to draw the reader's attention to the plots in Figure 13, where further smoothing of the natural frequency signals results in fewer false-negative/positive observations. It is also worth mentioning that temporal violation of the specified threshold does not physically attribute to the occurrence of damage, as damage is expected to be persistent in the system.

4 | EXPERIMENTAL VALIDATION: Z24 BRIDGE

This section investigates the problem of condition monitoring of the Z24 bridge. Several researchers have studied the Z24 bridge for different reasons, including:

1. Investigation of the feasibility of the identification using modal analysis,[49–51]
2. Studying the effect of the EOV on the structural dynamic characteristics and its mitigation for robust condition monitoring of the structure,[29,52,53]
3. Assessing the capability of proposed Vibration-based damage identification methods.[54–56]

The design and geometrical properties of the Z24 bridge are as follows, respectively:

1. a classical post-tensioned concrete two-cell box-girder bridge,
2. has a main span of 30 m and two side spans of 14 m as shown in Figure 14.

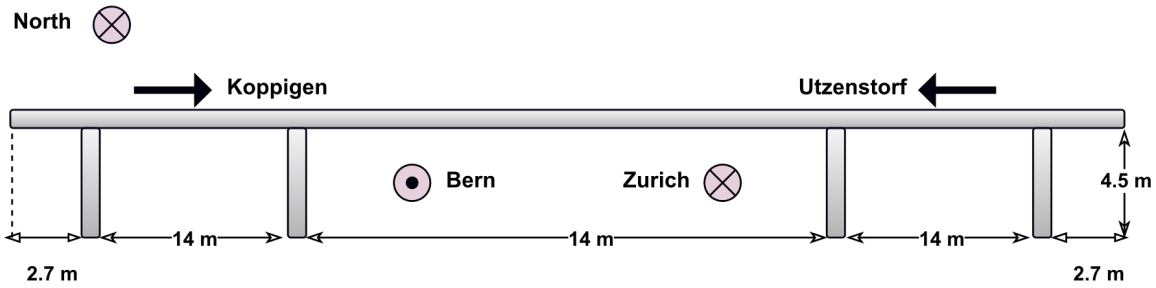

FIGURE 14 Z24 bridge geometry and location

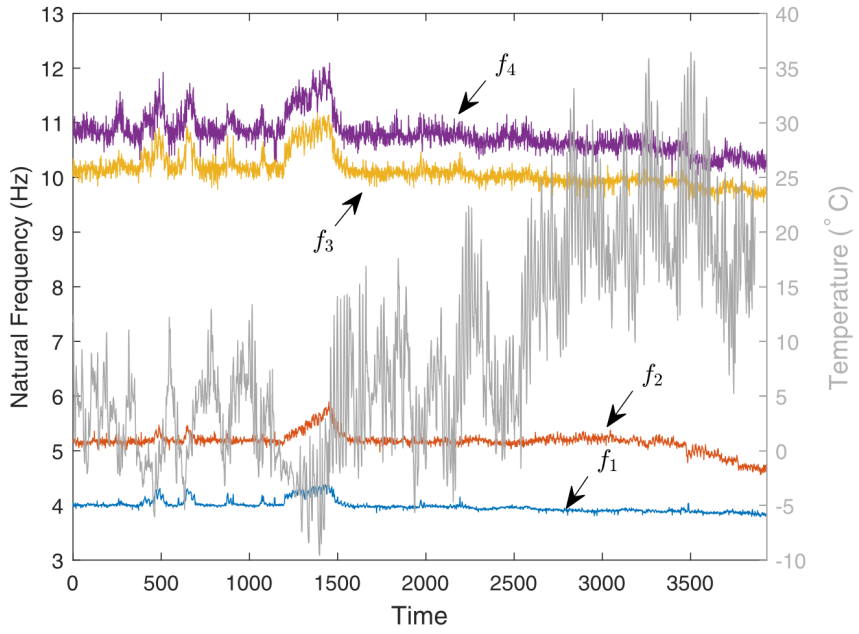

FIGURE 15 Right-to-left: The recorded temperature in the Z24 bridge deck; left-to-right: Obtained natural frequencies of the Z24 bridge

Some 16 accelerometers were used in different locations and directions to monitor the bridge dynamics. This led to obtaining the four lowest natural frequencies of the structure and the air temperature signals used for condition monitoring of the bridge in this section. However, there are some missing data points in the original dataset[†] displayed as NAN. Therefore, the rows corresponding to the NAN values in the concatenated matrix of the features and targets (i.e., the frequencies and temperature signals) were removed,[‡] as suggested in Shi et al.[42] Previous literature[57,58] has shown that the temperature at any location of the bridge can be strongly correlated (i.e., predicted) with the evolution of air temperature (e.g., using a moving average or convolutional neural networks); as a consequence, the exact location of temperature measurement is irrelevant. Figure 15 presents the temperature signal measured at the bridge deck[59] (right-to-left plot) and the four lowest natural frequencies (left-to-right plot) of the Z24 bridge with 3932 records. Note that the onset of damage begins at the time record 3470[60] and damage was introduced to the bridge structure gradually. More details about the Z24 bridge can be found in Maeck and De Roeck[61] and Reynders and De Roeck.[62]

Figure 16 shows the correlation between the frequencies and temperature. The plots indicate a linear dependency between the natural frequencies and temperature in the positive-temperatures region. This linear dependency is shown by the red dashed line. The similar slopes of the dashed lines indicate the existence of collinearity among the variables, further confirming the importance of considering interaction terms in a linear regression model. However, a more severe nonlinear fluctuation of the natural frequencies is evident in the region of freezing temperatures. The two following reasons might have contributed to this observation[29]:

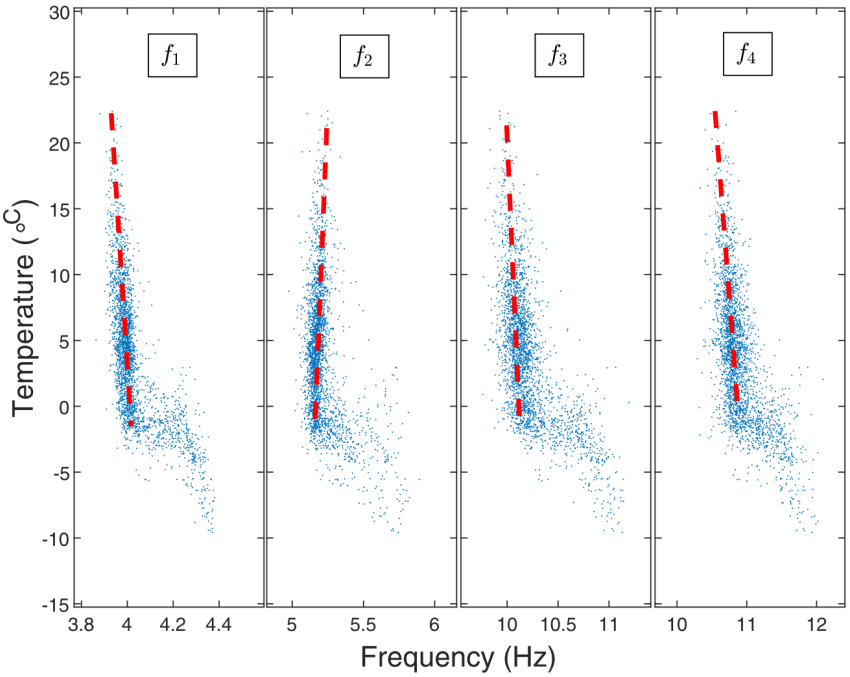

FIGURE 16 The scatter plot of the first four frequencies versus the temperature at the Z24 bridge

1. The freezing temperature might have frozen the soil and thus impacted the boundary conditions.
2. It might have also impacted Young's modulus of the constituent materials of the bridge.

As can be seen from the plots, there is a nonlinear dependency between the frequencies and temperature during a period of freezing temperature (roughly between 1300^{th} and 1500^{th} records).

Next, VMD decomposed the natural frequencies and temperature signals into two IMFs. The settings in the VMD were set similar to those of Section 3.1, except for α, which was set to 10 here as the data is less noisy compared to the numerical example of the spring-mass system. The decomposition results and their centre frequencies are depicted in Figures 17 and 18 for the temperature and natural frequency signals, respectively.

All the IMF_1 signals were also kept at zero centre frequency (a DC component) here. Next, the first 1000 records of all IMF_1 signals, corresponding to the healthy state of the structure, was used for training the MLAs of Table 1. Note that the second 1000 records were used as the validation set, and the remaining 1932 records were thus used as the test set.

Figure 19 shows the calculated $\overline{R}^2$ for the validation set of 1000 records, using all the MLAs. The five best models based on the obtained $\overline{R}^2$ are as follows: (1) Step-wise LR followed by interaction LR, (2) coarse trees, (3) coarse Gaussian SVM, (4) rational quadratic GPR, and (5) bagged trees. As seen from the bar lines, it is not as straightforward as the numerical section to decide which model is suitable for damage detection. However, we still stick to this hypothesis that the interaction LR is the best model for this study. This hypothesis will be further tested by conducting condition monitoring using all the best models. Note that although step-wise linear does slightly better than the interaction LR model, it is not preferable, following the same reason mentioned earlier. Therefore, it is hypothesised that the interaction LR model is the best candidate to establish the map. The following arguments also back up this hypothesis:

1. The original aim of training an MLA to predict temperature is not to perfectly fit the model on data. On the contrary, the model is preferred not to be generalisable to the case when damage occurs. It should also be noted that the UCL is obtained based on the prediction errors of the validation set, which represents the healthy state of the structure. Therefore, the threshold can be well adjusted even though the model might not perfectly fit on data.
2. The primary assumption behind obtaining a UCL for an R-chart is that the data (prediction errors) must follow a normal distribution. This assumption is compatible with the linear regression's normality assumption for the errors. Such an assumption might not hold for other MLAs; therefore, applying the R-chart concept might not fit well in those cases.

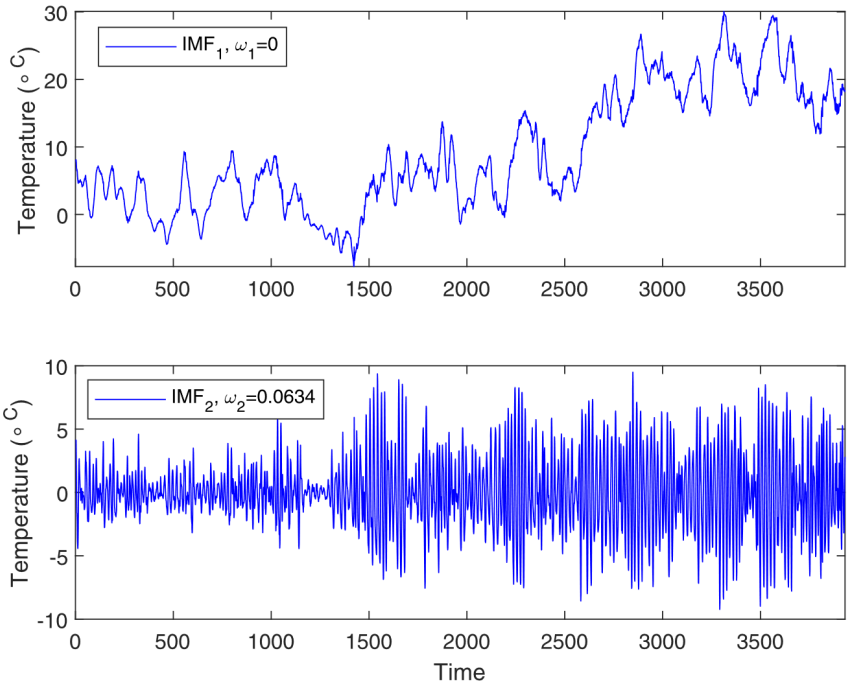

FIGURE 17 The decomposed temperature signal regarding the Z24 bridge along with its IMF centre frequencies

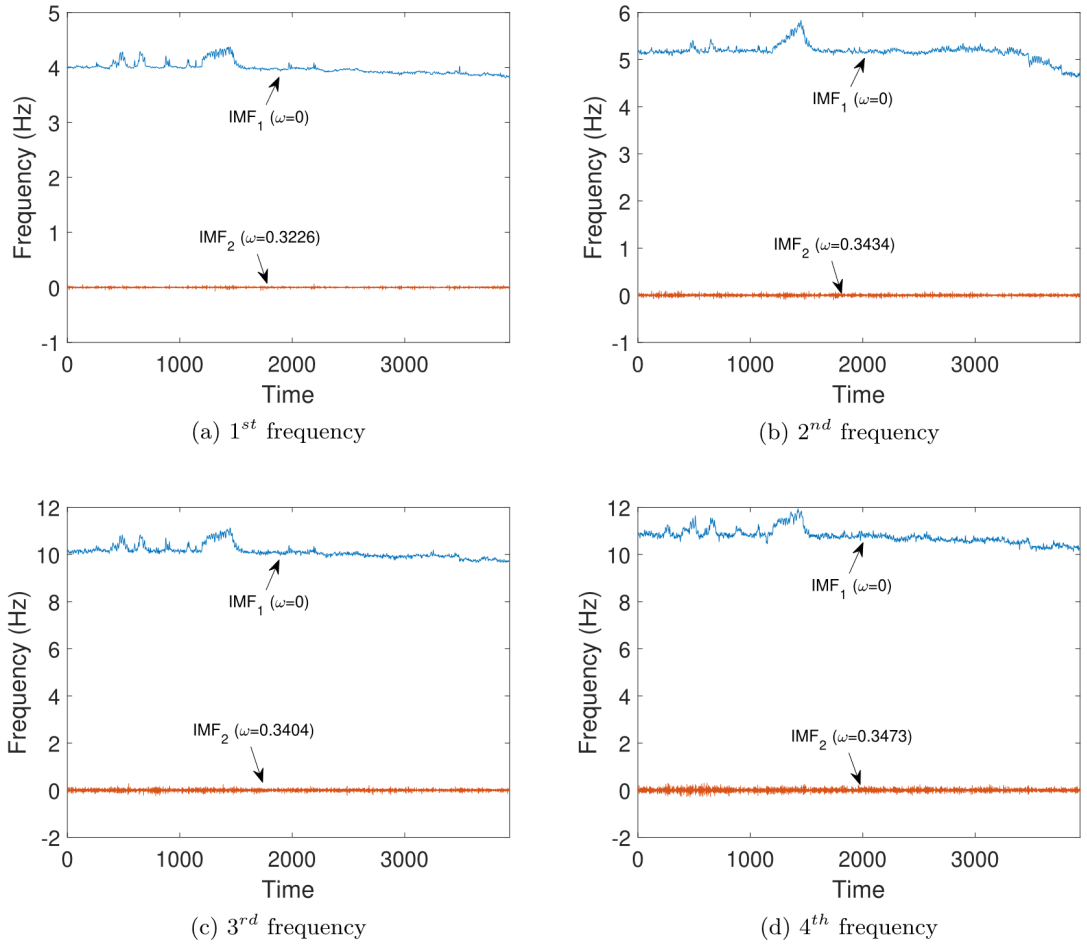

(a) 1^{st} frequency (b) 2^{nd} frequency

(c) 3^{rd} frequency (d) 4^{th} frequency

FIGURE 18 The decomposed natural frequencies of the Z24 bridge along with their centre frequencies

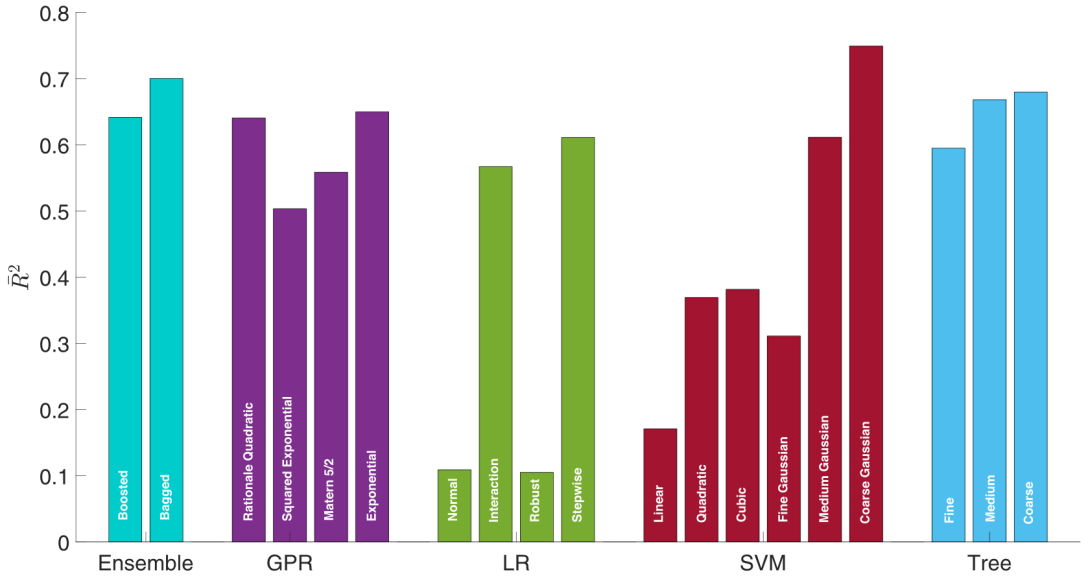

FIGURE 19 Calculated $\bar{R}^2$ for the validation set using different MLAs regarding the Z24 bridge

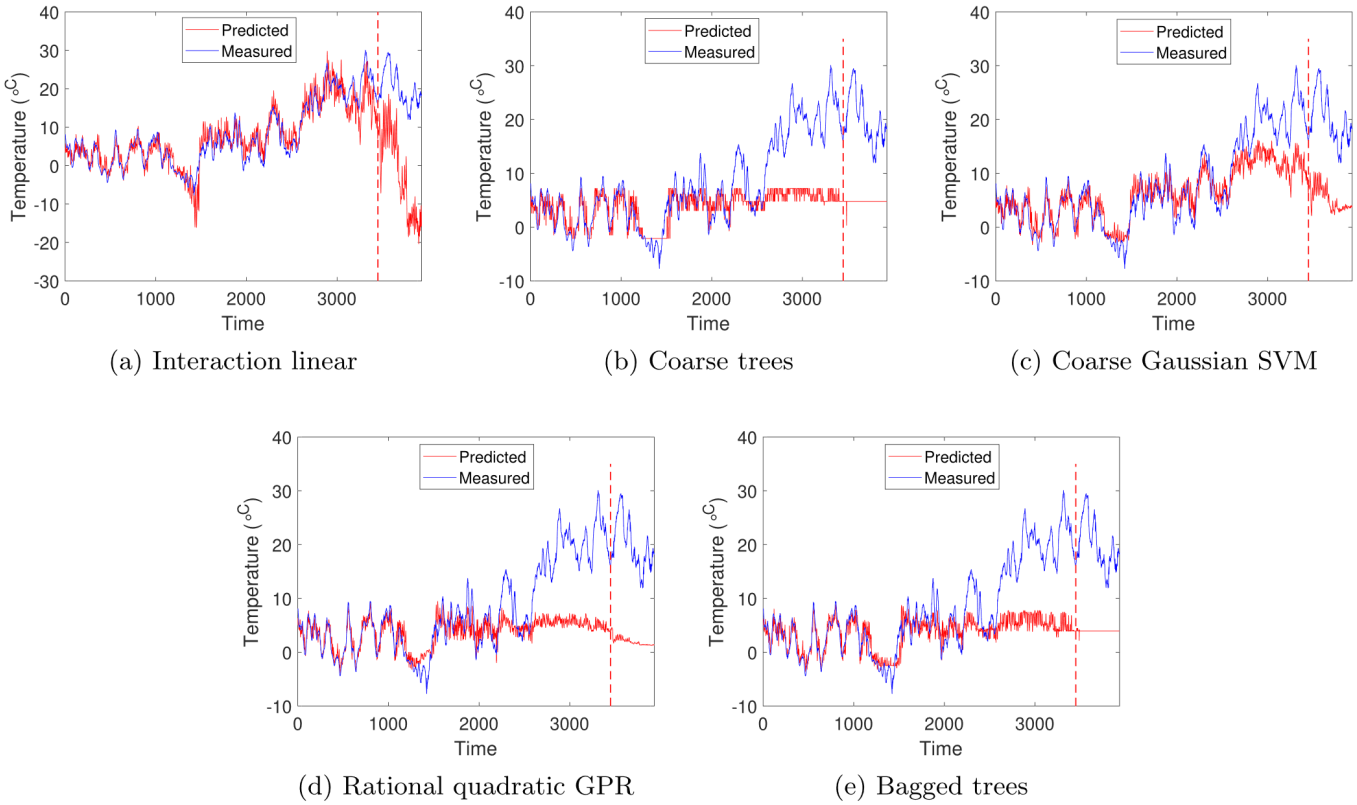

(a) Interaction linear (b) Coarse trees (c) Coarse Gaussian SVM

(d) Rational quadratic GPR (e) Bagged trees

FIGURE 20 The predicted and measured temperatures in the Z24 bridge deck using different trained MLAs

3. Adding a regularisation term will indeed increase the generalisability of the trained model. However, reiterated, a desirable model should not be generalisable for a damaged scenario. As such, using LR models with regularisation is not ideal for this study.

The plots of Figures 20 and 21 show respectively the prediction results and the errors associated with each prediction. Note that the vertical dashed line indicates the time of the introduction of damage (at 3470th record). As evident from the figures, the interaction LR model does far better than the other models. The interaction LR is successful in

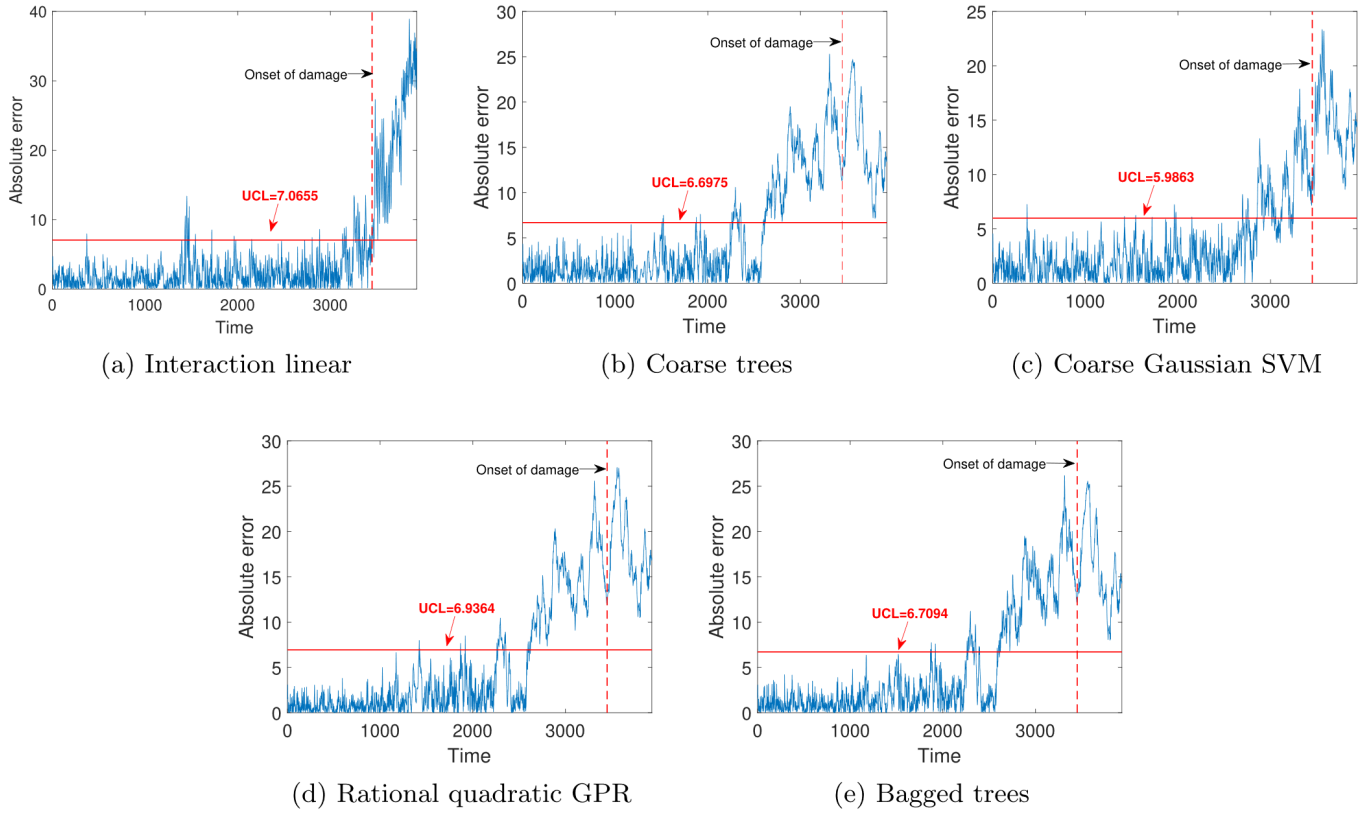

FIGURE 21 Condition monitoring results of the Z24 bridge using different trained MLAs (note differences in scale of y-axis in graphs)

TABLE 3 Parameters of the interaction LR model regarding the Z24 bridge

	Weight	β	SE	$\bar{t}_{\hat{\beta}_j}$	*p* value
Intercept	225.0351	β_0	326.7498	0.6887	0.4912
f_1	−216.7791	β_1	379.9556	0.5705	0.5684
f_2	1106.8506	β_2	140.4435	7.8811	0
f_3	−294.2782	β_3	137.8217	2.1352	0.0330
f_4	−201.4673	β_4	70.6365	2.8522	0.0044
$f_1\&f_2$	−235.9910	β_5	89.2753	2.6434	0.0083
$f_1\&f_3$	51.0128	β_6	21.8738	2.3321	0.0199
$f_1\&f_4$	79.6852	β_7	23.5135	3.3889	0.0007
$f_2\&f_3$	14.8717	β_8	31.0927	0.4783	0.6325
$f_2\&f_4$	−24.6224	β_9	23.3075	1.0564	0.2910
$f_3\&f_4$	0.4400	β_{10}	10.1979	0.04315	0.9656

capturing the interaction among frequency signals (as shown in Figure 16) due to the multiplicative interaction terms in the model, as shown in Equation (14). The results of the more complex MLAs though are not as good as the interaction LR model. One reason for this is the overfitting of more complex models on the training set. As such, although these models perform relatively well on the validation set, their performance on the test set is not acceptable. Next, we look at the parameters of the fitted interaction LR model to evaluate the importance of each term in the model.

Table 3 shows the parameters of the interaction LR model. As can be seen from the table, f_2 is the most important independent term in the model with $\bar{t}_{\hat{\beta}_j} = 7.8811$ followed by f_4 with $\bar{t}_{\hat{\beta}_j} = 2.8522$. Accordingly, f_1 is the least important feature with $\bar{t}_{\hat{\beta}_j} = 0.5705$. Note that again the obtained p value is a large value of 0.5684 in this case, indicating less

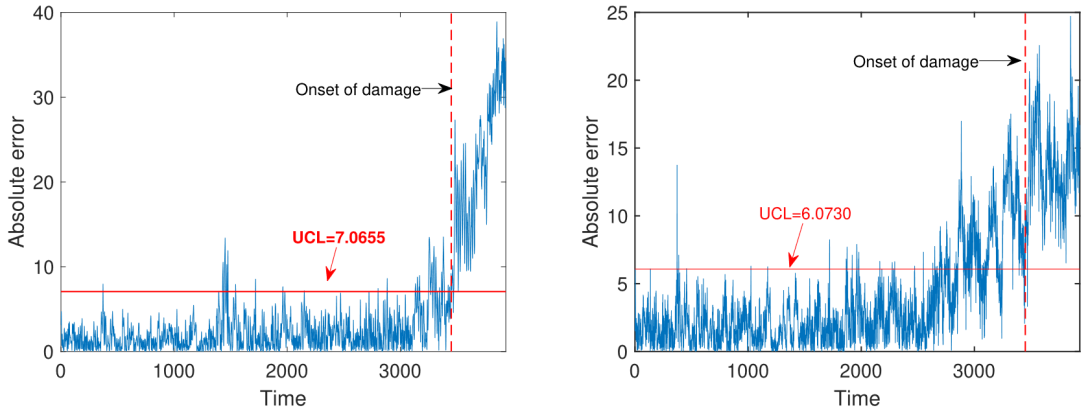

(a) With VMD (b) Without VMD

FIGURE 22 Condition monitoring results of the Z24 bridge with and without application of the VMD

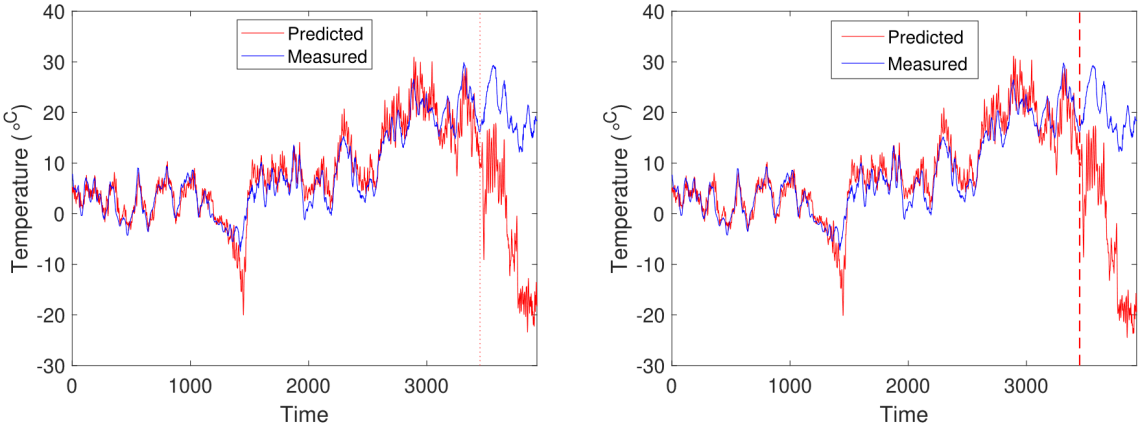

(a) $\alpha = 50$ (b) $\alpha = 100$

FIGURE 23 Prediction results of interaction LR model using different α in the VMD settings regarding the Z24 bridge

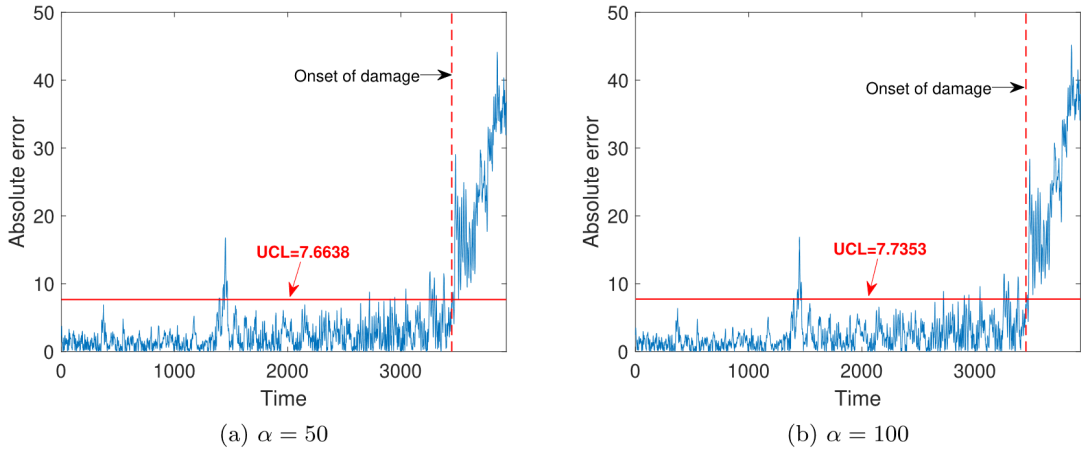

(a) $\alpha = 50$ (b) $\alpha = 100$

FIGURE 24 Errors associated with the prediction results of interaction LR model using different α in the VMD settings regarding the Z24 bridge

confidence on the role of f_1 in the prediction of temperature. Regarding the interaction terms, the term $f_1\&f_4$ has the most significant importance with $\bar{t}_{\hat{\beta}_j} = 3.3889$ followed by $f_1\&f_2$ with $\bar{t}_{\hat{\beta}_j} = 2.6434$. This again confirms that although f_1 is not a very important feature individually, its interaction with other terms can have a great influence on the prediction results. The least important interaction factor goes to the term $f_3\&f_4$ with $\bar{t}_{\hat{\beta}_j} = 0.04315$ and a large p value of 0.9656.

4.1 | Significance of using VMD

In this section, likewise to Section 3.4, the significance of employing the VMD in condition monitoring of the Z24 bridge is investigated. To this end, first, the results of the condition monitoring after the application of the VMD is compared against those without VMD. Following different values of α were selected to investigate their effect on the results.

Figure 22a,b shows respectively the results before and after the application of the VMD to the signals. As evident from the graphs of errors, employing the VMD plays a crucial role in improving the condition monitoring results. Again, the difference between the two results is highly significant.

Next, we specify different values of α in the VMD settings to investigate how increasing the denoising factor can affect the prediction results of the interaction LR model. Figures 23 and 24 show respectively the prediction results and errors associated with each prediction. It was noted, likewise to the spring-mass problem, that not only does not the increase of α compromise the fitness of the model, but it can also improve the condition monitoring results by increasing the resolution. As such, one may even try larger values of α and still expect to see decent results.

5 | COMPARISON WITH THE DIRECT REGRESSION-BASED STRATEGY

This section compares the results of the proposed inverse regression method against those obtained from a direct regression method. One can learn about the application of the direct approach from previous works.[6,23,63] The steps of the direct regression-based strategy are outlined as follows:

1. First, direct regression models are developed to establish maps from the temperature into each of the natural frequencies, that is, $T(t) \rightarrow f_i(t)$ for $i \in \{1, 2, 3, 4\}$. Note that, to this end, data from the healthy state of the structure is used for training. The results of this step are four maps that can be used to predict the future values of the frequencies using temperature as input.
2. The obtained maps are used to predict the future values of the frequencies corresponding to the second unknown state of the structure. The results of this step is the error associated with this prediction, shown as $\varepsilon_i = |f_i - \hat{f}_i|$ for $i = \{1, 2, 3, 4\}$.
3. Since four error signals are obtained from the previous step, the Shewhart (T^2) control chart is constructed to get a unique signal. Further details are provided here to keep the paper self-contained.

The Shewhart control chart is a conventional control charting model in statistical process control. The governing assumption of the model is that the observed variations inside the control limits, called fluctuations, are the results of accidental causes (EOV effects). In contrast, the variations lying outside the control limits, termed interruptions, result from assignable causes (damage). The model assumes that the observed fluctuations are inherent in the current process. It is thus uneconomical to investigate and eliminate these variations. However, the interruptions are external to the current process and, therefore, are generally economical to search for and eliminate the root causes.[64] The readers are referred to previous studies[38,65] for further details about the Shewhart control chart.

The last step of the above strategy requires the construction of a control chart. To this end, the Phase II Shewhart (T^2) control chart with individual observations (error values obtained from each mapping) is employed for performing condition monitoring.[38,65] The so-called T^2 chart is constructed as the second power of the Mahalanobis distance between each observation (error values) in the test set and the average point of the observations in the training set (the healthy state of the structure), as follows:

$$T^2 = \left(\mathbf{E}_{\text{test}} - \overline{\mathbf{E}}_{\text{train}}\right)' \mathbf{S}_{\text{train}}^{-1} \left(\mathbf{E}_{\text{test}} - \overline{\mathbf{E}}_{\text{train}}\right) \tag{17}$$

where $\mathbf{E}_{\text{test}}$ and $\mathbf{E}_{\text{train}}$ are the matrices of errors corresponding to the test and training sets. $\overline{\mathbf{E}}_{\text{train}}$ and $\mathbf{S}_{\text{train}}$ denote the mean value and covariance matrix of the training set, respectively. A UCL for the constructed chart can be obtained by considering p the number of variables and m the number of observations in the training set, as follows:

$$\text{UCL} = \frac{p(m+1)(m-1)}{m^2 - mp} \times F_{\alpha;\ p,m-p} \tag{18}$$

where $F_{\alpha;p,m-p}$ denotes the F-distribution with p and $m-p$ degrees of freedom and the significance level α. In this paper, α was set at 0.05 to obtain a 95% confidence interval for the calculated UCL.

The above procedure was applied to the condition monitoring problems of the spring-mass system and the Z24 bridge employing the most effective MLA for establishing the map between the frequencies and temperature signals, that is, the interaction LR model. Note that this reduces the models to normal LR models for the direct method due to the absence of interaction terms in the model. The obtained results are presented in Figure 25. As seen from the Figure 25a, it is evident that the direct method is not properly capable of condition monitoring of the spring-mass system. However, the results of the condition monitoring of the Z24 bridge using the direct approach are still compelling (Figure 25c).

Nevertheless, one can see a significant error in the time associated with the freezing temperature where the dependency between temperature and frequencies becomes nonlinear. However, this error is not as substantial regarding the results of the indirect method for the Z24 bridge. The reason is due to the effect of the interaction terms between features in the interaction LR model, which can describe this nonlinear dependency. Next, the results of the direct and indirect methods applied to the Z24 bridge are compared quantitatively. To this end, the F_1 score is obtained for each case, which is calculated through the following equation:

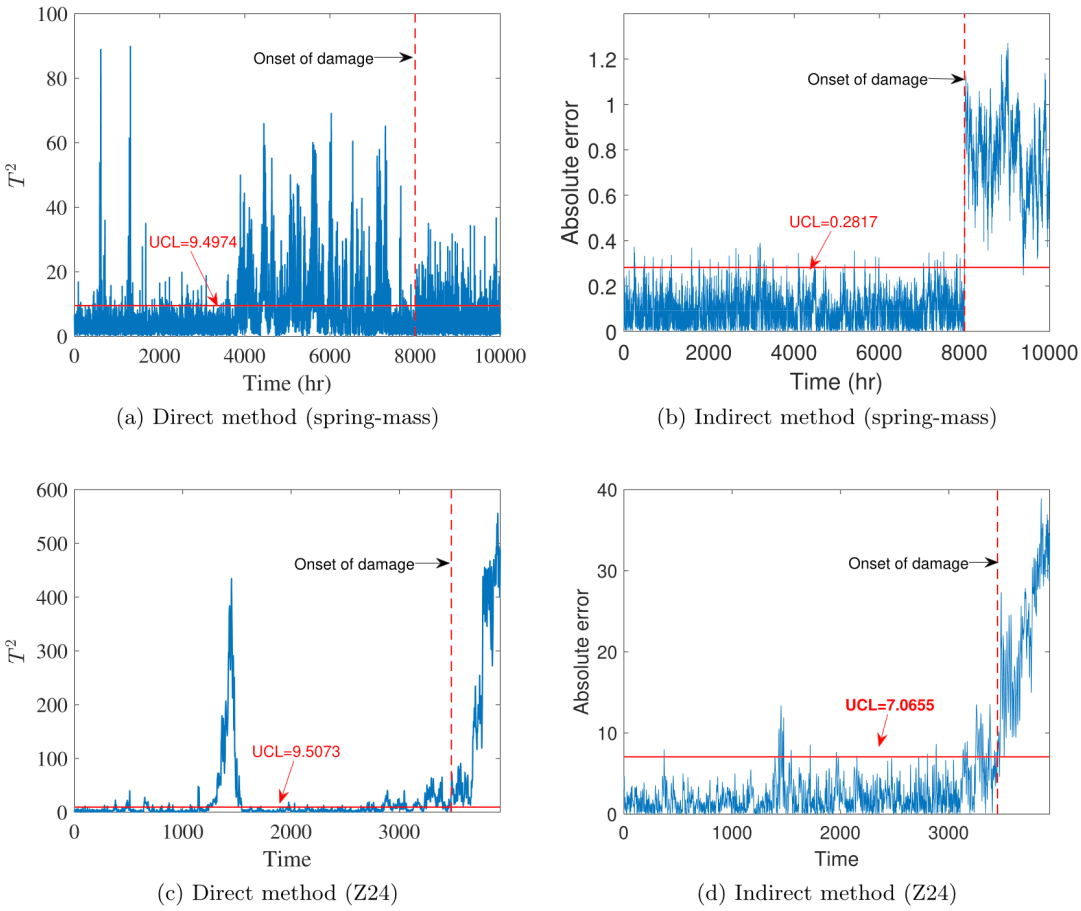

(a) Direct method (spring-mass) (b) Indirect method (spring-mass)

(c) Direct method (Z24) (d) Indirect method (Z24)

FIGURE 25 Condition monitoring results of the spring-mass system and the Z24 bridge employing the direct and the proposed indirect method

$$F_1 = \frac{tp}{tp + \frac{1}{2}(fn + fp)} \tag{19}$$

where tp, fp, and fn indicate the number of true positive, false positive, and false negative cases in the obtained results, respectively. Note that the lowest and the highest possible values of the F_1 score are 0 and 1, respectively. As such, a higher value of the F_1 indicates the better performance of a model, with 1 showing perfect results were achieved. The F_1 score was calculated for the test set, that is, from the 2000^{th} record onwards as for the Z24 bridge problem. This value was obtained respectively for the direct and indirect methods equal to 0.54 and 0.85, indicating the better performance of the proposed indirect method.

6 | CONCLUSIONS

A method for the long-term condition monitoring of civil infrastructures was proposed. It is known that the temperature modifies structural natural frequencies. Therefore, an inverse approach was proposed to predict temperature using the structural natural frequencies as input. The prediction error has been regarded as damage–sensitive feature. VMD was first employed to denoise signals and remove their seasonal patterns. Several MLAs were used to solve this study's numerical and experimental problems. The results show that the obtained interaction LR models perform relatively better than all the other examined MLAs. The following principal conclusions can be drawn based on the results:

- The linear dependency between the natural frequencies and temperature justifies using LR models for solving the regression problem of this paper. Nonetheless, a relatively nonlinear dependence between natural frequencies and the freezing temperature was evident from the data associated with the benchmark problem of the Z24 bridge. Further work needs to be done to confirm the appropriateness of the interaction LR models for condition monitoring of structures working under the icy situation.
- The regression line fitted to the frequency–temperature scatter plot indicates strong collinearity among natural frequency variations with respect to the temperature. Hence, considering interaction terms in a to-be-trained LR model is a must. The results further verified this conclusion.
- The interaction LR model is relatively a simple MLA; therefore, it can avoid overfitting the training set when a small number of data points is available for training. Moreover, the evaluation of the contribution parameter is made possible. For instance, the value of $\bar{t}_{\hat{\beta}_j}$ was used in this study to evaluate the importance of the independent and interactive features in the interaction LR models.
- The interaction terms in the model can successfully capture the nonlinear dependency between the temperature and frequency signals.

This paper used the value of $\bar{R}^2$ assessed on the validation set to evaluate a model's performance. It was noted that the value of $\bar{R}^2$, and therefore the model's fitness, was not compromised by using a more prominent denoising factor α in the VMD settings. On the contrary, improvements in the prediction results were evident in both the spring-mass and Z24 bridge problems.

The proposed algorithm can detect the progression of damage in the Z24 bridge. However, the main aim of this paper was not to distinguish different stages of damage in the system. If so, one may develop a multistage procedure where the model is trained on each step and tested in the proceeding stage. This way, one may identify the gradual progression of damage in the system. The primary aim of this paper was to develop a single model, as opposed to multiple models in the direct algorithm, for condition monitoring of civil infrastructures. As such, such a model is more flexible regarding its dependency on a single target value (temperature) and flexibility to the number of variables (natural frequencies) that may not be the case for the direct algorithm. Furthermore, alternative algorithms, such as the LARS algorithm, can be used to find parameters that significantly contribute to the temperature variation. Further work can be dedicated to investigating the effectiveness of such algorithms concerning the problem of this paper.

ACKNOWLEDGEMENT

The KU Leuven Structural Mechanics Section is acknowledged as the source of the data for Z24 bridge. Open access publishing facilitated by University of Technology Sydney, as part of the Wiley - University of Technology Sydney agreement via the Council of Australian University Librarians.

AUTHOR CONTRIBUTIONS

Mohsen Mousavi: Conceptualization; methodology; software; validation; formal analysis; investigation; resources; data curation; writing - original draft; visualization. **Amir H. Gandomi**: Validation; conceptualization; review & editing; supervision; project administration; funding acquisition. **Magd Abdel Wahab**: Data Curation; review & editing; supervision. **Branko Glisic**: Conceptualization; review & editing; supervision.

DATA AVAILABILITY STATEMENT

The data that support the findings of this study are available from the corresponding author upon reasonable request.

ENDNOTES

* A value close to 0.0428, obtained for the IMF_2 of the temperature signal.

† The four lowest natural frequencies and the air temperature signals.

‡ That's why no unit was specified for the time in the x-axis of the obtained figures.

REFERENCES

1. García Cava D, Avendaño-Valencia LD, Movsessian A, Roberts C, Tcherniak D. On explicit and implicit procedures to mitigate environmental and operational variabilities in data-driven structural health monitoring. *Structural Health Monitoring Based on Data Science Techniques*: Springer; 2022:309-330.
2. Liu C, DeWolf JT. Effect of temperature on modal variability of a curved concrete bridge under ambient loads. *J Struct Eng*. 2007;133(12):1742-1751.
3. Rainieri C, Magalhaes F, Gargaro D, Fabbrocino G, Cunha A. Predicting the variability of natural frequencies and its causes by second-order blind identification. *Struct Health Monit*. 2019;18(2):486-507.
4. Tatsis K, Ou Y, Dertimanis VK, Spiridonakos MD, Chatzi EN. Vibration-based monitoring of a small-scale wind turbine blade under varying climate and operational conditions. Part II: A numerical benchmark. *Struct Control Health Monit*. 2021;28(6):e2734.
5. Sousa Tomé E, Pimentel M, Figueiras J. Online early damage detection and localisation using multivariate data analysis: Application to a cable-stayed bridge. *Struct Control Health Monit*. 2019;26(11):e2434.
6. Magalhães F, Cunha A, Caetano E. Vibration based structural health monitoring of an arch bridge: from automated OMA to damage detection. *Mech Syst Signal Process*. 2012;28:212-228.
7. Cross EJ, Worden K, Chen Q. Cointegration: a novel approach for the removal of environmental trends in structural health monitoring data. *Proc R Soc A: Math Phys Eng Sci*. 2011;467(2133):2712-2732.
8. Cross EJ, Worden K. Cointegration and why it works for shm. *J Phys: Conf Ser*. 2012;382:12046.
9. Dao PB, Klepka A, Pieczonka L, Aymerich F, Staszewski WJ. Impact damage detection in smart composites using nonlinear acoustics–cointegration analysis for removal of undesired load effect. *Smart Materials Struct*. 2017;26(3):35012.
10. Li X, Qu W, Xiao L, Lu Y. Removal of temperature effect in impedance-based damage detection using the cointegration method. *J Intell Material Syst Struct*. 2019;30(15):2189-2197.
11. Dao PB, Staszewski WJ. Data normalisation for lamb wave–based damage detection using cointegration: a case study with single-and multiple-temperature trends. *J Intell Material Syst Struct*. 2014;25(7):845-857.
12. Tomé ES, Pimentel M, Figueiras J. Damage detection under environmental and operational effects using cointegration analysis—application to experimental data from a cable-stayed bridge. *Mech Syst Signal Process*. 2020;135:106386.
13. Michalak A, Wodecki J, Wyłomańska A, Zimroz R. Application of cointegration to vibration signal for local damage detection in gearboxes. *Appl Acoust*. 2019;144:4-10.
14. Mousavi M, Gandomi AH. Prediction error of Johansen cointegration residuals for structural health monitoring. *Mech Syst Signal Process*. 2021;160:107847.
15. Rainieri C, Reynders EPB. Pre-image reconstruction for compensation of environmental effects in structural health monitoring by kernel pca. In: Life cycle analysis and assessment in civil engineering: Towards an integrated vision: Proceedings of the Sixth International Symposium on Life-Cycle Civil Engineering (IALCCE 2018), 28-31 October 2018, Ghent, Belgium, Vol. 5 CRC Press; 2018:267.
16. Roberts C, Garcia D, Tcherniak D. A comparative study on data manipulation in PCA-based structural health monitoring systems for removing environmental and operational variations. In: Proceedings of the 13th International Conference on Damage Assessment of Structures Springer; 2020:182-198.
17. Liu A, Wang L, Bornn L, Farrar C. Robust structural health monitoring under environmental and operational uncertainty with switching state-space autoregressive models. *Struct Health Monit*. 2019;18(2):435-453.
18. Entezami A, Sarmadi H, Salar M, Behkamal A, Arslan AN, De Michele C. A novel structural feature extraction method via time series modelling and machine learning techniques for early damage detection in civil and architectural buildings. In: International Conference on Emerging Technologies in Architectural Design (ICETAD2019); 2019.
19. Worden K, Manson G, Fieller NRJ. Damage detection using outlier analysis. *J Sound Vibr*. 2000;229(3):647-667.

20. Dervilis N, Cross EJ, Barthorpe RJ, Worden K. Robust methods of inclusive outlier analysis for structural health monitoring. *J Sound Vibr*. 2014;333(20):5181-5195.
21. Ulriksen MD, Tcherniak D, Damkilde L. Damage detection in an operating Vestas v27 wind turbine blade by use of outlier analysis. In: 2015 IEEE Workshop on Environmental, Energy, and Structural Monitoring Systems (EESMS) Proceedings IEEE; 2015:50-55.
22. Mousavi M, Gandomi AH. A robust PCA-based framework for long-term condition monitoring of civil infrastructures. *Data Science in Engineering*, Vol. 9: Springer; 2022:79-85.
23. Mousavi M, Gandomi AH. Structural health monitoring under environmental and operational variations using MCD prediction error. *J Sound Vibr*. 2021;512:116370.
24. Yan A-M, Kerschen G, De Boe P, Golinval J-C. Structural damage diagnosis under varying environmental conditions-part I: a linear analysis. *Mech Syst Signal Process*. 2005;19(4):847-864.
25. Yan A-M, Kerschen G, De Boe P, Golinval J-C. Structural damage diagnosis under varying environmental conditions–part II: local PCA for non-linear cases. *Mech Syst Signal Process*. 2005;19(4):865-880.
26. Sen D, Erazo K, Zhang W, Nagarajaiah S, Sun L. On the effectiveness of principal component analysis for decoupling structural damage and environmental effects in bridge structures. *J Sound Vibr*. 2019;457:280-298.
27. Hsu T-Y, Loh C-H. Damage detection accommodating nonlinear environmental effects by nonlinear principal component analysis. *Struct Control Health Monit: Official J Int Assoc Struct Control Monit European Assoc Control Struct*. 2010;17(3):338-354.
28. Erazo K, Sen D, Nagarajaiah S, Sun L. Vibration-based structural health monitoring under changing environmental conditions using kalman filtering. *Mech Syst Signal Process*. 2019;117:1-15.
29. Peeters B, De Roeck G. One-year monitoring of the Z24-bridge: environmental effects versus damage events. *Earthq Eng Struct Dyn*. 2001;30(2):149-171.
30. Zhou HF, Ni YQ, Ko JM. Constructing input to neural networks for modeling temperature-caused modal variability: mean temperatures, effective temperatures, and principal components of temperatures. *Eng Struct*. 2010;32(6):1747-1759.
31. Kromanis R, Kripakaran P. Support vector regression for anomaly detection from measurement histories. *Adv Eng Inform*. 2013;27(4): 486-495.
32. Reilly J, Abdel-Jaber H, Yarnold M, Glisic B. Evaluating the coefficient of thermal expansion using time periods of minimal thermal gradient for a temperature driven structural health monitoring. In: Nondestructive Characterization and Monitoring of Advanced Materials, Aerospace, and Civil Infrastructure 2017, Vol. 10169 International Society for Optics and Photonics; 2017:1016929.
33. Ni YQ, Hua XG, Fan KQ, Ko JM. Correlating modal properties with temperature using long-term monitoring data and support vector machine technique. *Eng Struct*. 2005;27(12):1762-1773.
34. Ceravolo R, Coletta G, Miraglia G, Palma F. Statistical correlation between environmental time series and data from long-term monitoring of buildings. *Mech Syst Signal Process*. 2021;152:107460.
35. Han Q, Ma Q, Xu J, Liu M. Structural health monitoring research under varying temperature condition: a review. *J Civil Struc Health Monit*. 2021;11(1):149-173.
36. Shi H, Worden K, Cross EJ. A cointegration approach for heteroscedastic data based on a time series decomposition: an application to structural health monitoring. *Mech Syst Signal Process*. 2019;120:16-31.
37. Dragomiretskiy K, Zosso D. Variational mode decomposition. *IEEE Trans Signal Process*. 2013;62(3):531-544.
38. Thomas R. *Statistical Methods for Quality Improvement*. 2nd ed.: John Wiley & Sons; 2000.
39. Dragomiretskiy K, Zosso D. Variational mode decomposition. *IEEE Trans Signal Process*. 2014;62(3):531-544.
40. Zosso D. Matlab Central File Exchange. https://www.mathworks.com/matlabcentral/fileexchange/44765-variational-mode-decomposition; 2021.
41. Molnar C. *Interpretable Machine Learning, Chapter 4: Interpretable Models*: Lulu. com; 2020.
42. Shi H, Worden K, Cross EJ. A regime-switching cointegration approach for removing environmental and operational variations in structural health monitoring. *Mech Syst Signal Process*. 2018;103:381-397.
43. Moaveni B, Asgarieh E. Deterministic-stochastic subspace identification method for identification of nonlinear structures as time-varying linear systems. *Mech Syst Signal Process*. 2012;31:40-55.
44. Weather history download basel. https://www.meteoblue.com/en/weather/archive/export/basel_switzerland_2661604; 2020.
45. He W-Y, Ren W-X, Zhu S. Damage detection of beam structures using quasi-static moving load induced displacement response. *Eng Struct*. 2017;145:70-82.
46. Flom PL, Cassell DL. Stopping stepwise: why stepwise and similar selection methods are bad, and what you should use. In: Northeast SAS Users Group Inc 20th Annual Conference, Vol. 11; 2007.
47. Friedman J, Hastie T, Tibshirani R, et al. *The Elements of Statistical Learning, Chapter 3.2*, Vol. 1: Springer series in statistics New York; 2001.
48. Enders FB. Collinearity, Encyclopaedia Britannica. https://www.britannica.com/topic/collinearity-statistics. Accessed: July 15, 2022; 2013.
49. Peeters B, Ventura CE. Comparative study of modal analysis techniques for bridge dynamic characteristics. *Mech Syst Signal Process*. 2003;17(5):965-988.
50. Reynders E, De Roeck G. Reference-based combined deterministic–stochastic subspace identification for experimental and operational modal analysis. *Mech Syst Signal Process*. 2008;22(3):617-637.
51. Reynders E, Houbrechts J, De Roeck G. Fully automated (operational) modal analysis. *Mech Syst Signal Process*. 2012;29:228-250.

52. Reynders E, Wursten G, De Roeck G. Output-only structural health monitoring in changing environmental conditions by means of nonlinear system identification. *Struct Health Monit*. 2014;13(1):82-93.
53. Langone R, Reynders E, Mehrkanoon S, Suykens JohanAK. Automated structural health monitoring based on adaptive kernel spectral clustering. *Mech Syst Signal Process*. 2017;90:64-78.
54. Maeck J, Peeters B, De Roeck G. Damage identification on the Z24 bridge using vibration monitoring. *Smart Materials Struct*. 2001; 10(3):512.
55. Teughels A, De Roeck G. Structural damage identification of the highway bridge Z24 by fe model updating. *J Sound Vibr*. 2004;278(3): 589-610.
56. Reynders E, De Roeck G. A local flexibility method for vibration-based damage localization and quantification. *J Sound Vibr*. 2010; 329(12):2367-2383.
57. Abdel-Jaber H, Glisic B. Systematic method for the validation of long-term temperature measurements. *Smart Mater Struct*. 2016;25(12): 125025.
58. Oh BK, Park HS, Glisic B. Prediction of long-term strain in concrete structure using convolutional neural networks, air temperature and time stamp of measurements. *Automation Construct*. 2021;126:103665.
59. Bull LA, Rogers TJ, Wickramarachchi C, Cross EJ, Worden K, Dervilis N. Probabilistic active learning: An online framework for structural health monitoring. *Mech Syst Signal Process*. 2019;134:106294.
60. Sarmadi H, Entezami A, Salar M, De Michele C. Bridge health monitoring in environmental variability by new clustering and threshold estimation methods. *J Civil Struct Health Monit*. 2021;11:629-644.
61. Maeck J, De Roeck G. Description of Z24 benchmark. *Mech Syst Signal Process*. 2003;17(1):127-131.
62. Reynders E, De Roeck G. Vibration-based damage identification: The Z24 benchmark; 2014.
63. Kullaa J. Damage detection of the Z24 bridge using control charts. *Mech Syst Signal Process*. 2003;17(1):163-170.
64. Cheremisinoff NP. *Condensed Encyclopedia of Polymer Engineering Terms*: Butterworth-Heinemann; 2001.
65. Montgomery DC. *Introduction to Statistical Quality Control, chapter 10*. 4th ed.: John Wiley & Sons; 2001.

How to cite this article: Mousavi M, Gandomi AH, Abdel Wahab M, Glisic B. Monitoring onsite-temperature prediction error for condition monitoring of civil infrastructures. *Struct Control Health Monit*. 2022;29(12):e3112. doi:10.1002/stc.3112